The behaviour of continuous beams in reinforced concrete

(Results of experimental and theoretical investigation)

Th. Monnier
I.B.B.C.

Summary

This paper describes both experimental and theoretical research performed on continuous beams in reinforced concrete. A general survey of the behaviour of that kind of structures is discussed at first. The tests on two-span beams are fully described. An analysis-procedure is taken into consideration next, where the influence of the shear force can be taken into account. Finally, the calculated and measured results are compared.

The investigation described leads to the conclusion, that the shear-effect must be taken into account in order to get the good agreement between measured and calculated data.

CONTENTS

Notations

A	area of tensile reinforcement
A'	area of compressive reinforcement
A_a	total area of the stirrups crossed by an inclined crack
A_t	area of one stirrup
a	distance between the supports and the nearest point load
a_1	distance defined in Fig. V-1
B	cross sectional area of a concrete compressive diagonal
b	width of rectangular section
b_o	width of rectangular section or web thickness of flanged beam
c	vertical concrete cover on a bar of the tensile reinforcement
d'	distance from extreme compressive fibre to centroid of tensile reinforcement
d_s	distance from the center of a corner bar to the corner of the cross-section
E	modulus of elasticity
E_a	modulus of elasticity of steel (reinforcement)
E'_{bo}	modulus of elasticity in the origin of the concrete stress-strain diagram
(EI)	bending stiffness
$(EI)_o$	bending stiffness in the uncracked state
$(EI)_g$	bending stiffness in the cracked state $(= \frac{\Delta M}{\Delta \varkappa})$
$(EI)_{gd}$	stiffness in the cracked state including the influence of shear
f	deflection
f_m	deflection at mid-span
$\bar{f}_m$	permissible deflection according to the GBV 1962 (Dutch Code for the concrete constructions)
Δf_t	increase of the deflection due to shear
G	modulus of shear
$(GB)_o$	stiffness for shear deformation in the uncracked state
$(GB)_g$	stiffness for shear deformation in the cracked state
h	distance from extreme compressive fibre to centroid of tensile reinforcement
h_t	total depth of the cross-section
I_{bo}	moment of inertia of an uncracked cross-section including the quantity of steel
K	quality of the concrete (for K 300, σ'_w = 300 kg/cm^2)
k	reduction factor for the steel stress in the stirrups
$k'_d h$	= d' = distance from extreme compressive fibre to centroid of compressive reinforcement

$k_x h$	= x = depth of the neutral axis
$k_z h$	= z = lever arm
ℓ	span length
ℓ_i	length of a beam element
$\Delta\ell$	crack distance
M	bending moment
M_i	average moment in a beam region i
M_u	yield moment
M_v	moment in the spans (M_{v_1} ; M_{v_2} moments at the points of loading)
M_s	moment at the interior support
M_{uv}	= M_u for the reinforcement in the spans
M_{us}	= M_u for the reinforcement at the interior support
M_r	cracking moment
ΔM	total bending moment less M_r
N_a	resultant steel tensile force
N'_a	resultant steel compressive force
N'_b	resultant concrete compressive force
n	number of bars of the tensile reinforcement
n_o	ratio of modulus of elasticity of steel to that of concrete $\left(= \frac{E_a}{E'_{bo}}\right)$
P	point load
Q	total live load on the continuous beam
Q_u	theoretical failure load ($M_s = M_{us}$; $M_v = M_{uv}$)
Q_{uv}	theoretical load Q, by which $M_v = M_{uv}$ and $M_s < M_{us}$
Q_{us}	theoretical load Q, by which $M_s = M_{us}$ and $M_v < M_{uv}$
Q_s	service load ($= Q_u/\gamma$)
R	reaction force
T	shear force
T_a	tensile force in stirrups due to shear
T_b	compressive force due to shear in a concrete diagonal
T_r	shear force at M_r in the region of the inclined crack
t	horizontal center to center distance of the stirrups
W_{bo}	section modulus of an uncracked cross-section including the quantity of steel
w	crack width
$\bar{w}_{max}$	permissible maximum crack width according to the GBV 1962

x	depth of neutral axis
z	lever arm
$\emptyset$	diameter in mm of a bar of the reinforcement or stirrup
α	inclination of stirrups with respect to axis of beam or ratio a/ℓ
β	angle between concrete compressive diagonal and axis of beam
γ	safety factor (= 1.8)
ε_a	strain of tensile reinforcement
ε'_a	strain of compressive reinforcement
ε'_b	concrete compressive strain
ε'_{bu}	max. concrete compressive strain at failure (= 3.5‰ according to the GBV 1962)
ζ	ratio M_s/M_v
$\varkappa$	measured average curvature or calculated curvature due to bending
$\Delta\varkappa$	total curvature less the curvature at cracking moment
$\Delta\varkappa_t$	increase of the curvature due to shear
λ_e	ratio M_{v1}/M_s
λ_u	ratio M_{uv}/M_{us}
ν	Poisson's ratio
ξ	ratio $\Delta\varkappa_t/\Delta\varkappa$
σ_a	stress in tensile reinforcement
σ'_a	stress in compressive reinforcement
σ_{ae}; σ'_{ae}	yield stress of tensile reinforcement and compressive reinforcement, respectively
σ_b	tensile stress (in bending) of concrete
σ'_{bu}	max. concrete compressive stress (= 0.6 σ'_w according to the GBV 1962)
σ'_w	concrete compressive stress determined on cubes
τ_o	shearing stress
$\tau_{o,s}$	shearing stress at inclined cracking
ψ	shearing strain
ω_o	percentage of tensile reinforcement (= $100\,\frac{A}{bh}$ or $100\,\frac{A}{b_o h}$)
ω'_o	percentage of compressive reinforcement (= $\frac{100A'}{bh}$)
ω_t	stirrup reinforcement ratio (= $\frac{A_t}{bt \sin\alpha}$)

1. Statically indeterminate structures in reinforced concrete

1.1 Introduction

In accordance with the principles of elementary limit-design there is considerable freedom in distributing the reinforcement over the various critical sections in a statically indeterminate reinforced concrete structure. Starting from a desired collapse load, any reinforcement arrangement can be chosen which will still just enable equilibrium to be achieved for a given collapse mechanism.

However, reinforced concrete structures present the complication that, with the procedure outlined above, it cannot be presupposed that an acceptable structure with regard to service-load conditions will always be obtained. Under service-load there are also certain requirements to be fulfilled. The maximum crack width is not allowed to exceed certain permissible values, and the same applies to the deflection. These requirements restrict the considerable amount of freedom in the choice of reinforcement arrangement that would exist on the basis of limit-design alone.

The main-object of the investigation to be described here is to determine these limiting factors more specifically. This paper contains a survey of the research work done so far and presents the results obtained.

To begin with, the investigation concentrates on continuous beams constructed of reinforced concrete. For these structures the limits (e.g., ζ_1 and ζ_2) will be determined within which the ratio of support reinforcement to span reinforcement must remain in order to fulfil the service-load requirements. With these limits and some supplementary rules as given data it is a simple matter to design continuous beams by limit design which are acceptable also with regard to the service-ability.

The very simple case of a beam continuous over a number of supports for instance (see Fig. 1), can be treated as follows. Basing oneself on the statically determinate main system of the spans (i.e., assuming each span to be independent and freely supported), the total quantity of reinforcement required is calculated as $A_{tot.}$ cm^2. The closing line of the bending moment diagram can now be so drawn that $M_{support}/M_{span} = \zeta$. If ζ is situated between the above-mentioned limits ζ_1 and ζ_2, then the beam will also fulfil the service load requirements. In that case the quantity of reinforcement to be installed over the supports is $\frac{\zeta A_{tot.}}{1 + \zeta}$ cm^2, and the quantity to be installed in the mid-span regions is $\frac{A_{tot.}}{1 + \zeta}$ cm^2.

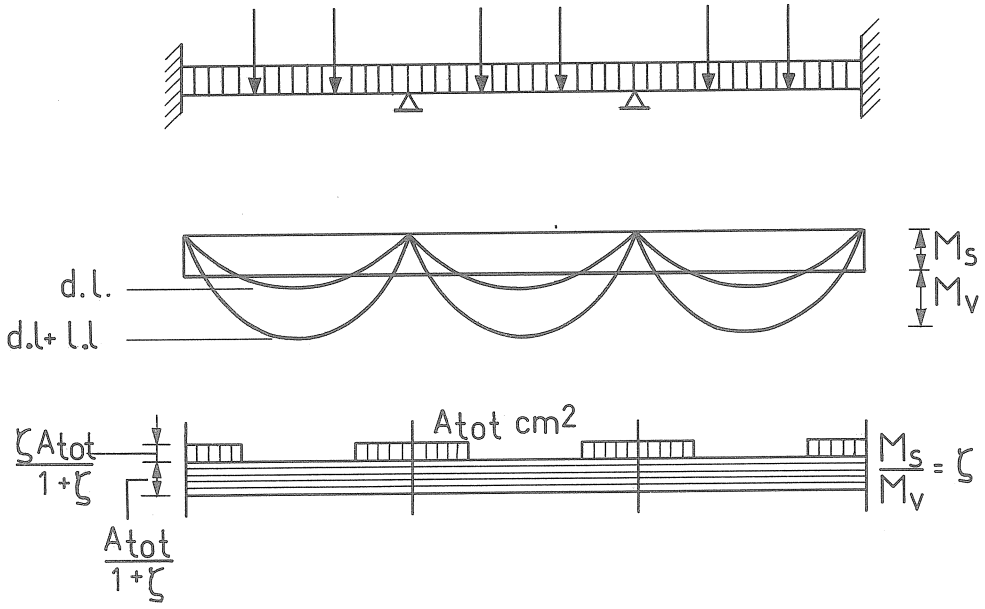

Fig. 1. Scheme of a continuous beam.

In general, it will be possible to adapt the reinforcement rather more closely to the moment diagram than has been indicated in the diagram in Fig. 1. On the other hand sufficient bond length must be provided.

1.2 Survey of the investigation performed

The investigation concerning the behaviour of statically indeterminate reinforced concrete structures began with a study of the bending stiffness of reinforced concrete. The moment-curvature (M-$\varkappa$) diagram was determined in experimental research. The M-$\varkappa$ diagram of reinforced concrete is especially dealt with in a separate publication.*) Next, experimental work was undertaken on continuous beams. Besides, a method of analysis was programmed for performing the calculations by computer.

The purpose of this computer programme was to obtain a computational aid whereby the behaviour of statically indeterminate structures could be fully analysed. The advantages are obvious. The importance of various factors affecting the results can thereby easily and quickly be investigated. Having regard to the object of the present investigation,

*) The moment-curvature relation of reinforced concrete; Heron, vol. 17 (1970), no. 2

namely, the determination of the limits referred to in the introduction, it was virtually indispensable also to have such a computational aid at one's disposal. This is because the said limits have to be determined by fully analysing a certain number of cases.

In the present publication the behaviour of statically indeterminate structures in general will first be discussed, and then the following subjects will be considered:

- experimental research on two-span continuous beams;
- the computation programme and the analysis principles employed in it (including the M-$\varkappa$ diagram of reinforced concrete);
- comparison of the measured and the calculated results with regard to the continuous beams.

The investigation has at present reached a point where the calculations are being performed from which the limits to be established can be inferred.

1.3 General discussion of the behaviour of statically indeterminate reinforced concrete beams

For a proper understanding of the behaviour of such reinforced concrete structures it is of course necessary to know the flexural stiffness of reinforced concrete. This property can be determined by measuring the relation between bending moment and curvature (i.e., the M-$\varkappa$ diagram) in the region of constant bending moment of a beam subjected to a four-point flexural loading test. These measurements showed that the moment-curvature relation can be approximated very well by three straight lines. Fig. 2 gives a number of M-$\varkappa$ diagrams for various percentages of tensile reinforcement. The first branch of the diagram relates to uncracked concrete. At the moment M_r the effect of cracking is manifested. The stiffness then decreases. In the M-$\varkappa$ diagram the horizontal third branch is reached when the yield stress develops in the tensile reinforcement.

The consequences of this with regard to the behaviour of, for example, a continuous beam are evident. This is shown in Fig. 3. On the vertical axis is plotted the load 2P, while the values of the moments M are plotted in the horizontal direction. The two thinly drawn lines indicate the elastic moments: the span moment on the left, the support moment on the right. The thicker lines relate to the moments that actually occurred.

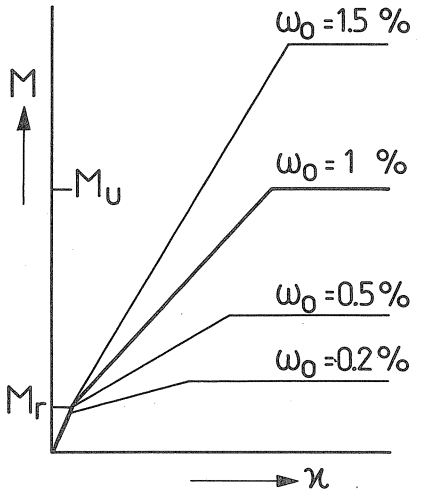

Fig. 2. Some examples of M-$\varkappa$ diagrams.

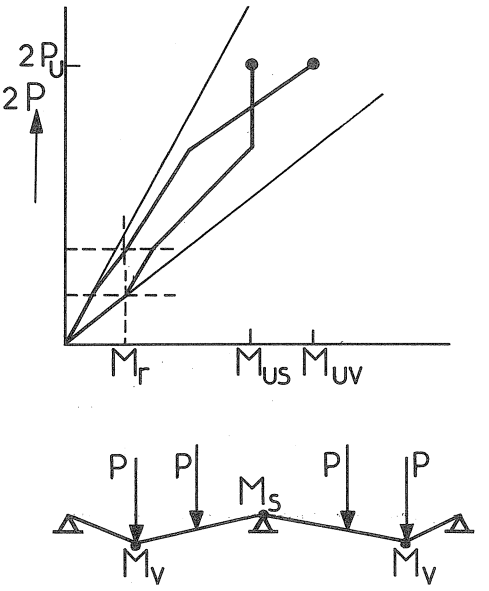

Fig. 3. Resdistribution of moments in a 2-span continuous beam.

With increasing load, the beam at first remains uncracked. There is no reason why the distribution of the bending moments should deviate from the elastic values: in the diagram the relevant lines do in fact coincide. If the support moment is the first to reach the value M_r (the 'cracking moment'), then the reduction of stiffness associated with the cracking results in a redistribution of the moments. With further load increase the support moment increases less rapidly. To maintain the requisite equilibrium, the moment in the span now becomes relatively larger. The cracking in the mid-span region has a compensating effect upon this. Thereafter the distribution of the moments depends entirely on the then existing stiffness ratio between the region of the positive and the region of the negative moments. In the diagram the yield moment is first attained over the support. No further increase in the support moment can occur with further load increase. A plastic hinge has developed. The beam sections in the mid-span region must now alone cope with the required increase in the moment. When the tensile reinforcement in the spans finally also begins to yield, the collapse mechanism shown in Fig. 3 develops. The load cannot

now be further increased; the beam collapses and fractures where the rotational capacity of a plastic hinge is reached (see Fig. 4).

Starting from that collapse mechanism, the structure can also be analysed in accordance with the elementary limit design concepts. As will be apparent from the experimental research that was conducted, it is not at all necessary that the yield moments be simultaneous attained at the critical sections. Yielding can quite permissibly occur somewhere in the structure before there is any question of a "Mechanism" having developed. In normal structures the plastic hinges are able to provide sufficient rotational capacity for this. Hence, in general, in determining the ultimate strength, it is permissible to base oneself on a distribution of forces for which the requisite equilibrium is possible. For reinforced concrete continuous beams this means that the ratio of span reinforcement to support reinforcement can be arbitrarily chosen; this choice will not impair the safety of the structure in question.

The reinforced concrete structure must, however, also fulfil the serviceability-conditions: maximum crack width and deflection. These two aspects undoubtedly constitute a restriction of the great measure of freedom in the distribution of reinforcement that the limit design method in itself affords. As said before little is known, however, concerning the extent of that restriction.

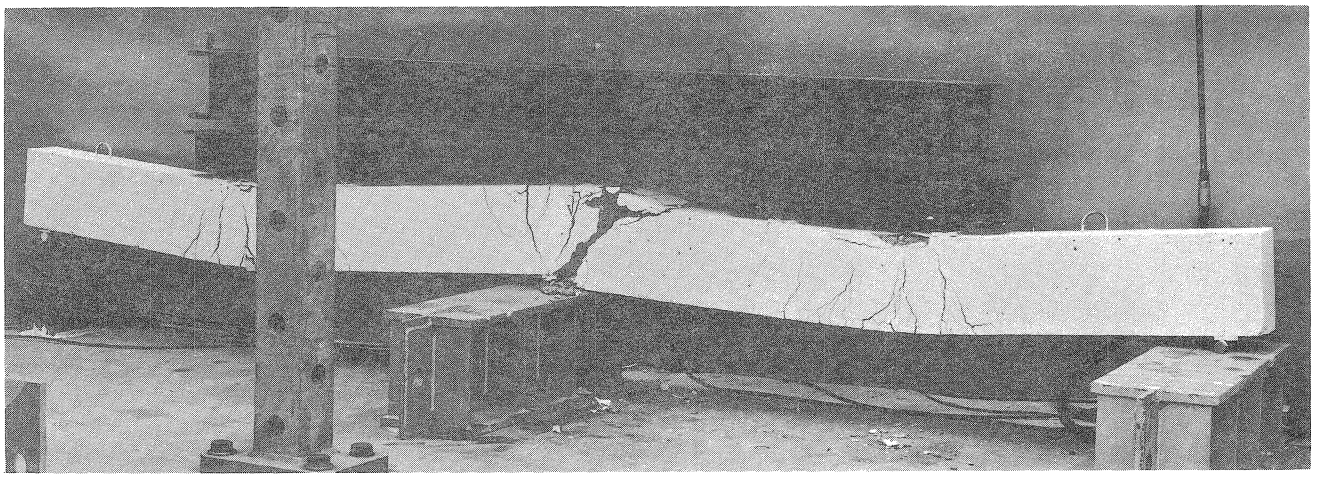

Fig. 4. A 2-span beam after failure.
Tensile reinforcement in the spans 2Ø6 + 2Ø10 ≡ 0.61%
Tensile reinforcement at the interior support 2Ø6 + 1Ø10 ≡ 0.38%

2. Experimental investigation of two span continuous beams

2.1 General information on the test beams

The beams which were investigated had an overall length of 420 cm and were tested as continuous beams on three supports, the two spans being each 200 cm in length. The cross-sectional dimensions were b = 15 cm and h_t = 26 cm. The effective depth both for the top and for the bottom reinforcement was h = 23.6 cm. In all the test beams the longitudinal reinforcement consisted of 12 mm diameter deformed bars (see Fig. 5) of steel grade QR 40 ($\sigma_{ae\ min.}$ = 4000 kg/cm^2). The stress-strain diagrams for these bars are plotted in Fig. 6.

In the cross-section of each beam there were always two and three longitudinal bars as tensile reinforcement and compressive reinforcement respectively, or vice versa. The longitudinal reinforcement remained constant over the entire length of the beam. Details of the reinforcement for each beam (the beams are marked B_1, B_2, B_3 and B_4) are given in the table accompanying the cross-section shown in Fig. 7.

The beams were provided with stirrups of 8 mm diameter, consisting of the same grade of steel as the longitudinal reinforcement. These stirrups were made by welding four bars together (see Fig. 7) and served also for accurately fixing the longitudinal bars in the formwork. The stirrup reinforcement was the same in all the test beams, as shown in Fig. 8.

The strength of the concrete was of the order of magnitude of 300 kg/cm^2. In Table 1 these strengths, together with the other properties of the concrete, are given for each beam separately. The data of 20 cm cubes will be used as cube strength σ'_w of the concrete.

2.2 Description of the investigation

The beams described in the foregoing were tested as two-span continuous beams, i.e., on three supports, the spans being each 200 cm in length. The loading consisted of two point loads applied to each span. In all cases these loads were spaced at 50 cm centre-to-centre and were disposed symmetrically with respect to mid-span. The test arrangements are shown schematically in Fig. 9.

The beams B_1, B_2 and B_4 were loaded with two equal loads P applied to each span. The bending moment diagram for this case is presented in Fig. 9a. In the case of the beam B_3, however, one of the two forces acting on

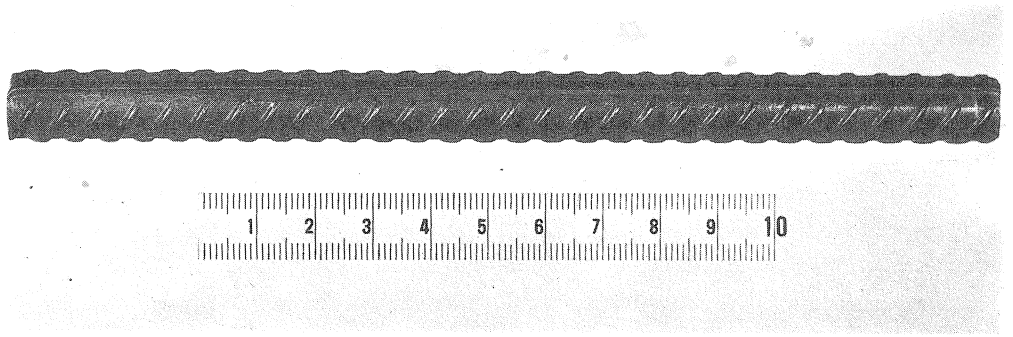

Fig. 5. Deformed Hi-Bond bar ∅ 12 mm.

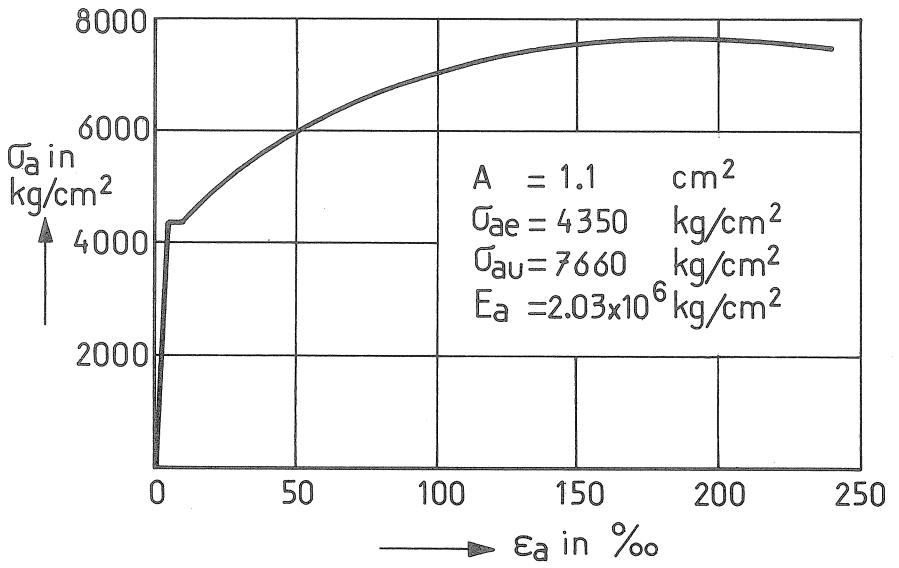

Fig. 6. Stress-strain diagram of the bar ∅ 12 mm.

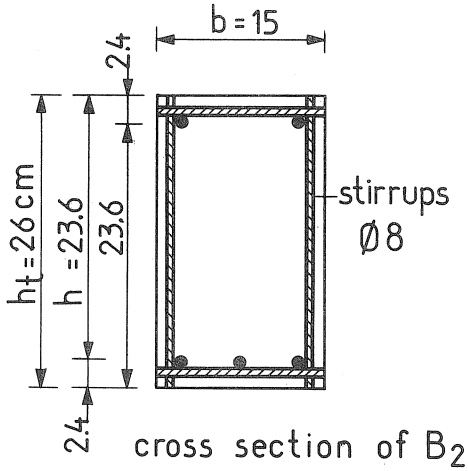

beam	tensile reinf. in the spans	tensile reinf. at the interior support	perc. of reinf. $\omega_o = \frac{100A}{bh}$
B_1	2Ø12	3Ø12	2Ø12 ≡
B_2	3Ø12	2Ø12	0.64%
B_3	3Ø12	2Ø12	3Ø12 ≡
B_4	3Ø12	2Ø12	0.96%

Fig. 7. Typical details of the test beams.

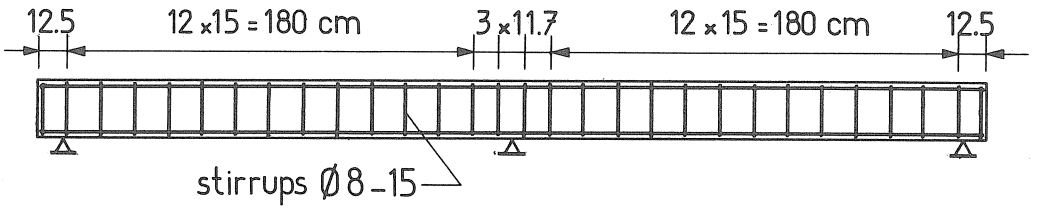

Fig. 8. The stirrup reinforcement.

calculation stirrup reinforcement					
beam no.	max. shear force T_u at ultimate in kg (from table 2)		lever arm z_e, z_m in cm	From Appendix V: $\omega_t = \frac{T_u}{b.z.\sigma_{ae}}$ in ‰	
	end support	middle support		end support	middle support
B_1	2839	5978	21.9, 21.6	1.99	4.24
B_2, B_4	4216	6322	21.6, 21.9	3.04	4.51
B_3	3619	7027	21.6, 21.9	2.62	5.00
All beams provided with:				Ø8-15 ≡ 4.49	Ø8-11.7 ≡ 5.75

Table 1. Strength properties of the concrete.

beam number	1	2	3	4	5	6	7
	cube strength	compressive strength	prism strength	splitting strength	flexural (tensile) strength	modulus of elasticity	bulk density
	kg/cm^2	kg/cm^2	kg/cm^2	kg/cm^2	kg/cm^2	kg/cm^2	kg/dm^3
B_1	310/327	345	267	28.7	45.1	3.20×10^5	2.30
B_2	313/325	324	299	26.5	39.5	3.19×10^5	2.31
B_3	308/348	339	266	27.9	44.1	3.35×10^5	2.32
B_4	330/383	373	-	29.8	47.8	3.37×10^5	2.33
average	315/346	345	277	28.2	44.1	$3.28\ 10^5$	2.32

1) measured on four 20 cm cubes, pressed between 3 mm cardboard, respectively four 15 cm cubes, pressed without cardboard

2) pressed between 2 steel plates 10×10×3 cm

3) 1 prism 10×10×30 cm

4) average of two 15 cm cubes

5) average of three 10×10×30 cm prisms, loaded according the 3-point bending test with a span length of 20 cm

6) two 10×10×30 cm prisms

concrete composition:

. Portland cement A Enci	325 kg/m^3
. water/cement ratio	0.57
. aggregate/cement ratio (dry weight)	6.0
. hardened by 20°C and 65% R.H.	

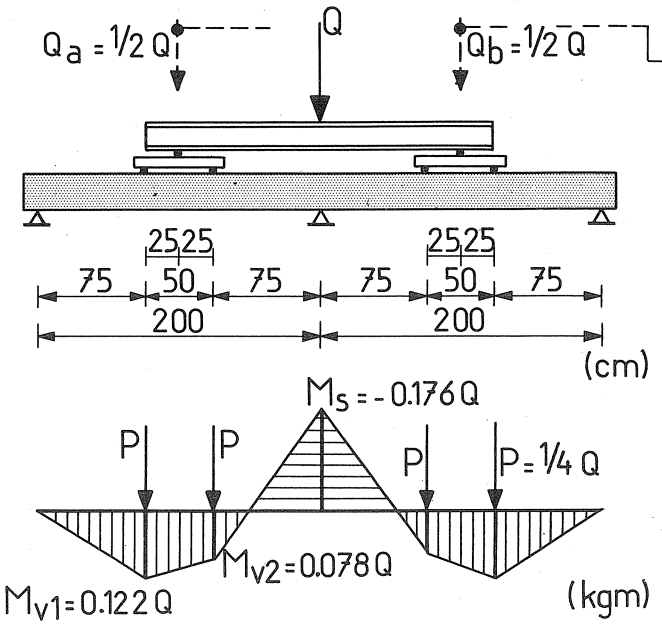

(Q_a and Q_b are only applied to beam B_4 as separate loads, see fig. 11)

Loading system of B_1, B_2 and B_4.

Fig. 9a.

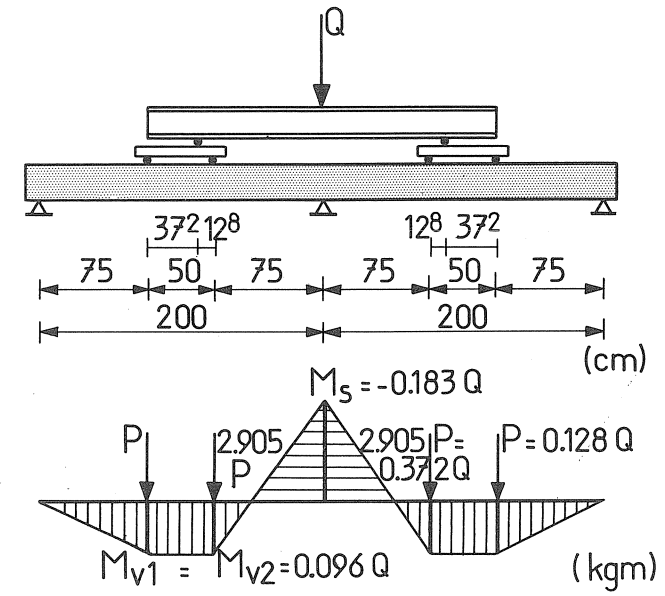

Loading system of B_3.

Fig. 9b.

Fig. 9. Loading systems and the actual areas of moment diagrams.

Table 2. Strength properties of the test beams .

beam	elastic moments (kgm)			reinforcement		yield moments available for live load (kgm) [1]			theoretical failure- and yield load (kg) [2]				
	M_s	M_{v1}	$\lambda_e = \frac{M_{v1}}{M_s}$	support	span	M_{us}	M_{uv}	$\lambda_u = \frac{M_{uv}}{M_{us}}$	Q_u	Q_{uv}	Q_{us}	$\frac{Q_{uv}}{Q_u}$	$\frac{Q_{us}}{Q_u}$
B_1	0.176 Q	0.122 Q	0.690	3Ø12	2Ø12	3141	2129	0.678	17634	17519		0.993	
B_2	0.176 Q	0.122 Q	0.690	2Ø12	3Ø12	2108	3161	1.500	21076		11978		0.568
B_3	0.183 Q	0.096 Q	0.525	2Ø12	3Ø12	2108	3161	1.500	21291		11522		0.541
B_4	0.176 Q	0.122 Q	0.690	2Ø12	3Ø12	2108	3161	1.500	21076		11978		0.568
	0.176 Q	0.309 Q	1.755	(one span loaded, $Q_a = Q_b = Q = 2P$)				1.500	10538	10231		0.971	

[1] yield moment for tensile reinforcement 3Ø12: M_u = 3187 kgm
" " " " " 2Ø12: M_u = 2155 kgm

[2] simultaneous yielding over the support (M_s) and in the span (M_{v1}):
$Q_u = 0.667\ M_{us}\ (8\lambda_u + 3)$ beam B_1, B_2 and B_4
simultaneous yielding over the support (M_s) and the span (M_{v2}):
$Q_u = 0.594\ M_{us}\ (8\lambda_u + 5)$ beam B_3
} see Appendix IV

Assuming the stiffness (EI) is constant along the whole length of the beam, then the load at which the tensile reinforcement starts to yield is:

$$Q_{uv} = \frac{M_{uv}}{0.122} \quad \text{for beam } B_1 \ (M_{v1} = M_{uv})$$

$$Q_{us} = \frac{M_{us}}{0.176} \quad \text{for beam } B_2 \text{ and } B_4 \ (M_s = M_{us})$$

$$Q_{us} = \frac{M_{us}}{0.183} \quad \text{for beam } B_3 \ (M_s = M_{us})$$

one span, namely, the force applied nearest the central support, was about 2.9 times as large as the other. The elastic distribution of the bending moment thus obtained comprised a zone of constant moment between the two loads on a span (see Fig. 9b).

For all the test beams the elastic bending moments at the significant sections associated with the loading case concerned are given in Table 2. The theoretical analysis is presented in Appendix I. The same table also indicates the positioning of the reinforcement and the magnitude of the yield moments associated with it. The method of calculating the yield moments is set forth in Appendix II. All the moments indicated are values caused by external loading or, alternatively, available for resisting external loading. In all cases the investigation was based on the beam inclusive of the bending moments due to dead weight (see Fig. 10).

In beam B_1 the support tensile reinforcement consists of three 12 mm bars and the tensile reinforcement in the spans of two 12 mm bars, this arrangement being adopted as the best possible adaptation of the reinforcement to the elastic distribution of the moments (see Table 2). As already stated, in all the beams the span reinforcement and the support reinforcement was continued throughout the length of the beam. In the beams B_2, B_3 and B_4 the reinforcement was reversed in relation to B_1: the support reinforcement consisted of two 12 mm bars and the span reinforcement of three 12 mm bars. In beam B_2 the reinforcement was therefore just reversed in relation to the magnitude of the elastic moments. In B_3 there was relatively even less support reinforcement, inasmuch as the two forces on a span of this beam were not equal. Finally, in so far as the position and magnitude of the loading were concerned, beam B_4 was in the same circumstances as beam B_2. The loading applied to the beams B_1, B_2 and B_3 was increased by increments, in the usual way, until failure occurred; in the case of B_4 the loading was, in addition, subjected to alternations at each increment.

These alternations, which were commenced after the cracking moment had been reached, proceeded in accordance with a "shake-down analysis" pattern:

Suppose that at the load increment under consideration a total load Q was acting on the beam. First this total load was applied (i.e., to both spans) and then removed again. Next, half the load Q was placed on one of the spans and removed. Then the other span was loaded with $\frac{1}{2}$ Q and un-

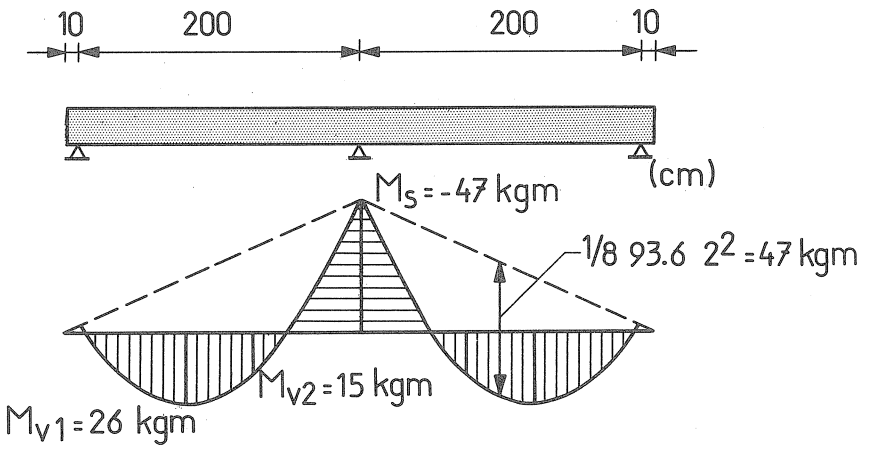

Fig. 10. The test beam including the above mentioned moments caused by the dead weight (= 93.6 kg/m') of the beam has always been taken as zero point of the measurements.
The weight of the loading equipment was, however, taken into account as applied loading.

loaded. Finally, the total load Q was again applied to the whole beam. One cycle of alternations is shown schematically in Fig. 11.

This cycle was repeated during the testing of the beam until, at the load increment in question, a steady state was attained. This steady state was recognisable by the fact that the measured reactions at the supports due to full load Q were found to have the same value after the application of a particular cycle of load alternations as they had before such application. During the cycles, precautions were taken to prevent lifting of the end support of the non-loaded span.

For measuring the reactions, load cells were installed under the three supports of all the test beams. From these observations the actually occurring distribution of the bending moments had, inter alia, to be calculated. The said load cells were disposed on an assembly of steel plates and adjusting screws, whereby the height of the bearings could be accurately adjusted. For this purpose, too, dial gauges were installed, by means of which, with the aid of a stand, any changes in the level of the supports in relation to the (immovable) floor of the testing laboratory were measured. During the execution of the test these displacements were always corrected; it was thus ensured that the supports could not undergo any displacement in relation to each other. Fig. 12 shows the arrangements at an end support.

2.2.1 Observations made

In the zero position (twice) and furthermore after the application of each load increment the following data were measured and recorded:

- The height of the bearings in relation to the floor of the testing laboratory. If this dimension, after the load had been increased, was found to have changed to such an extent that the three supports were no longer all at the same level, corrections to restore this were applied. For this reason the loads were always increased in small increments.
- The magnitude of the bearing reactions. In the zero position and during the first few load increments the heights of the bearings were so adjusted that the magnitude of the reactions corresponded to the elastic (calculated) values. Thus no secondary stresses were produced in the beams, despite the fact that they were not "ideal" beams in the sense of being absolutely straight.

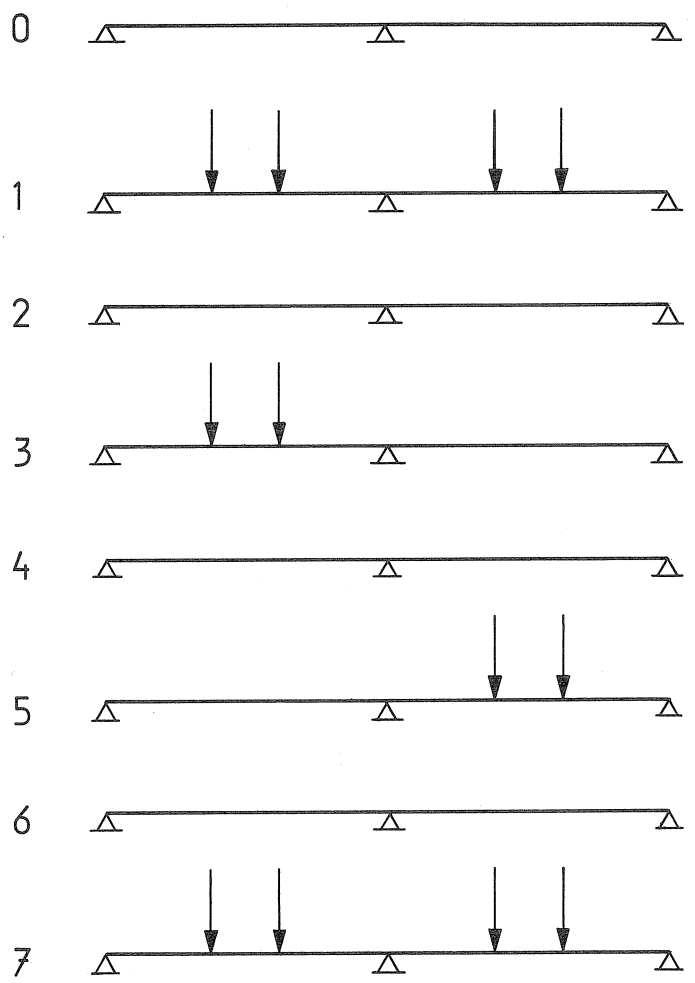

Fig. 11. Stages in the course of one load alternation cycle.

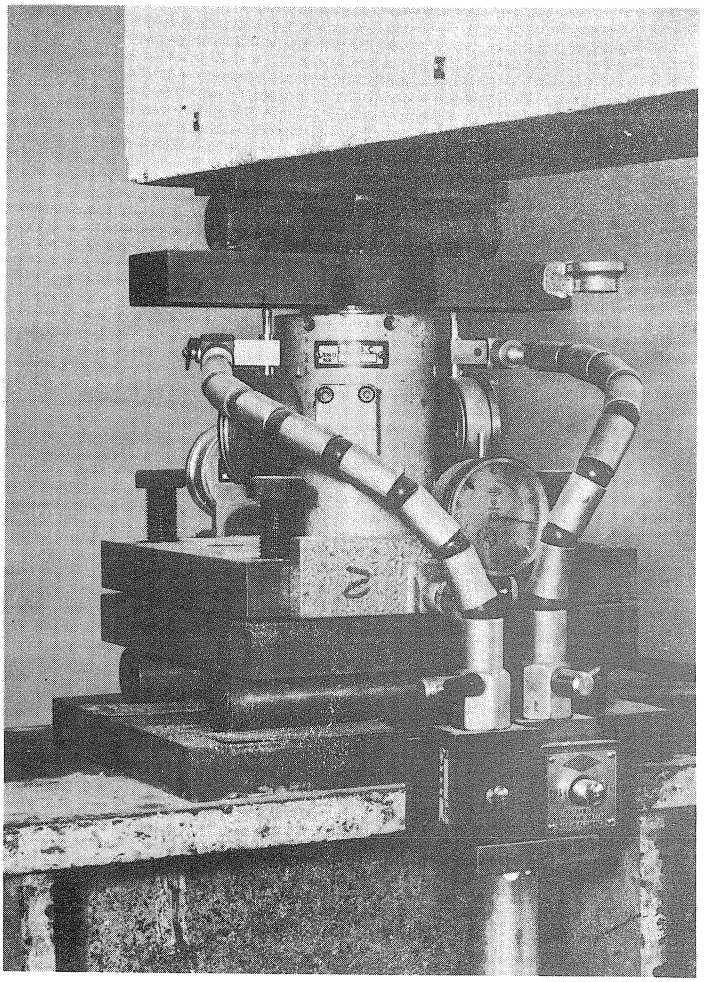

Fig. 12. View of an adjustable end support with a load cell to measure the reaction force at the support.

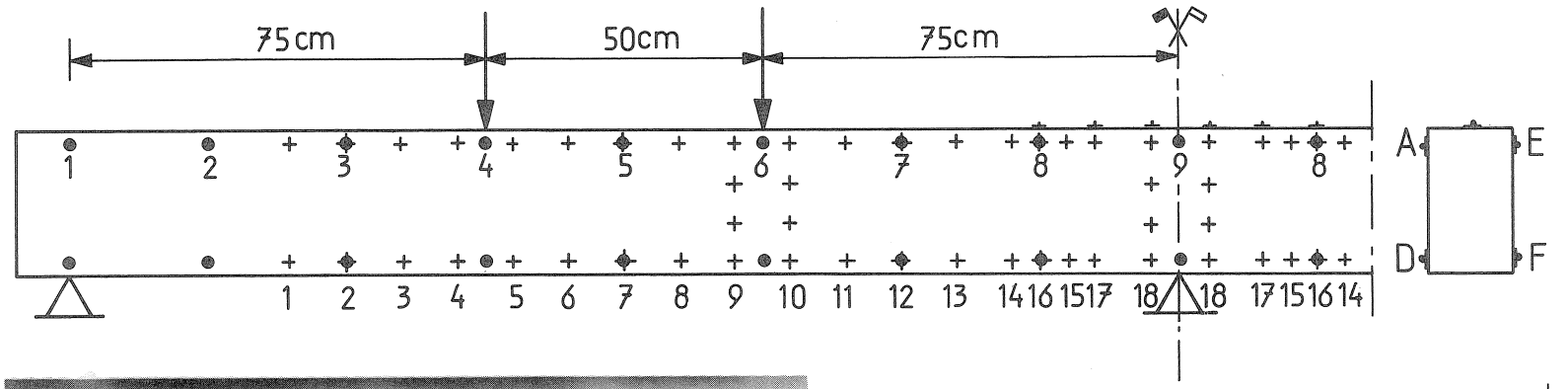

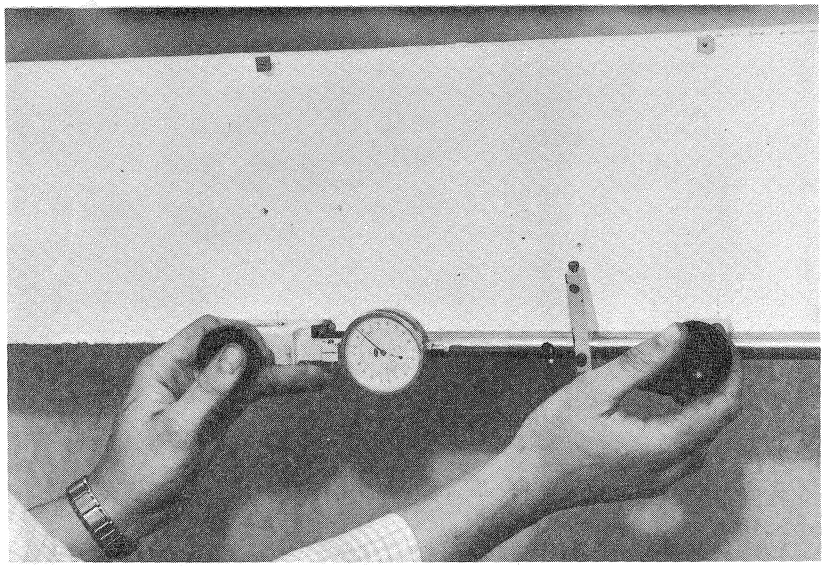

Fig. 13. The strain gauge lay-out and the demountable strain gauge used.

. measuring points, gauge length 25 cm

\+ measuring points, gauge length 10 cm

- The mid-span deflections in both spans. These deflections were measured with the aid of a levelling instrument.
- The tensile and compressive strains at the level of the tensile and compressive reinforcement respectively, i.e., 2.4 cm from the bottom or from the top of the beam. These measurements were performed with a demountable strain gauge applied to both sides of each beam and along the entire length thereof; the gauge length was 25 cm.

Also, over a considerable proportion of the length the beams were provided, on one side, with measuring points for a smaller demountable strain gauge, the gauge length in this case being 10 cm. These measurements were not performed after each load increment had been applied.

Fig. 13 shows the location of the measuring positions on the beams.

In the case of beam B_4 all the above-mentioned observations were obtained when a steady-state condition had been attained after the load alternations had been applied. This was done both with the beam fully loaded and with loading on one span only. Before alternation was started, the bearing reactions, the deflection and the strain, the latter measured on a 25 cm gauge length only, were determined.

The measurements on each beam took six working days to carry out.

2.2.2 Results of the measurements

In the first place, the following data are presented:

- the measured distribution of the moments in the beams; the maximum span moment and the support moment are given;
- the mid-span deflections.

The results of the measurements relating to these quantities have been plotted against the corresponding total load Q on the beam. For the beams B_1 to B_4 they are successively presented in Figs. 14, 16, 18 and 20. The calculation of the moment distribution from the bearing reactions is given in Appendix III.

A different method of plotting the support moments and maximum moments in the spans against the corresponding loads has also been employed. In Figs. 25 to 29 (at the end of this chapter) the moments calculated from the bearing reactions and divided by the calculated yield moment in the region concerned have been plotted against the total load acting on the beam divided by the calculated failure load. The calculation of the failure load is presented in Appendix IV.

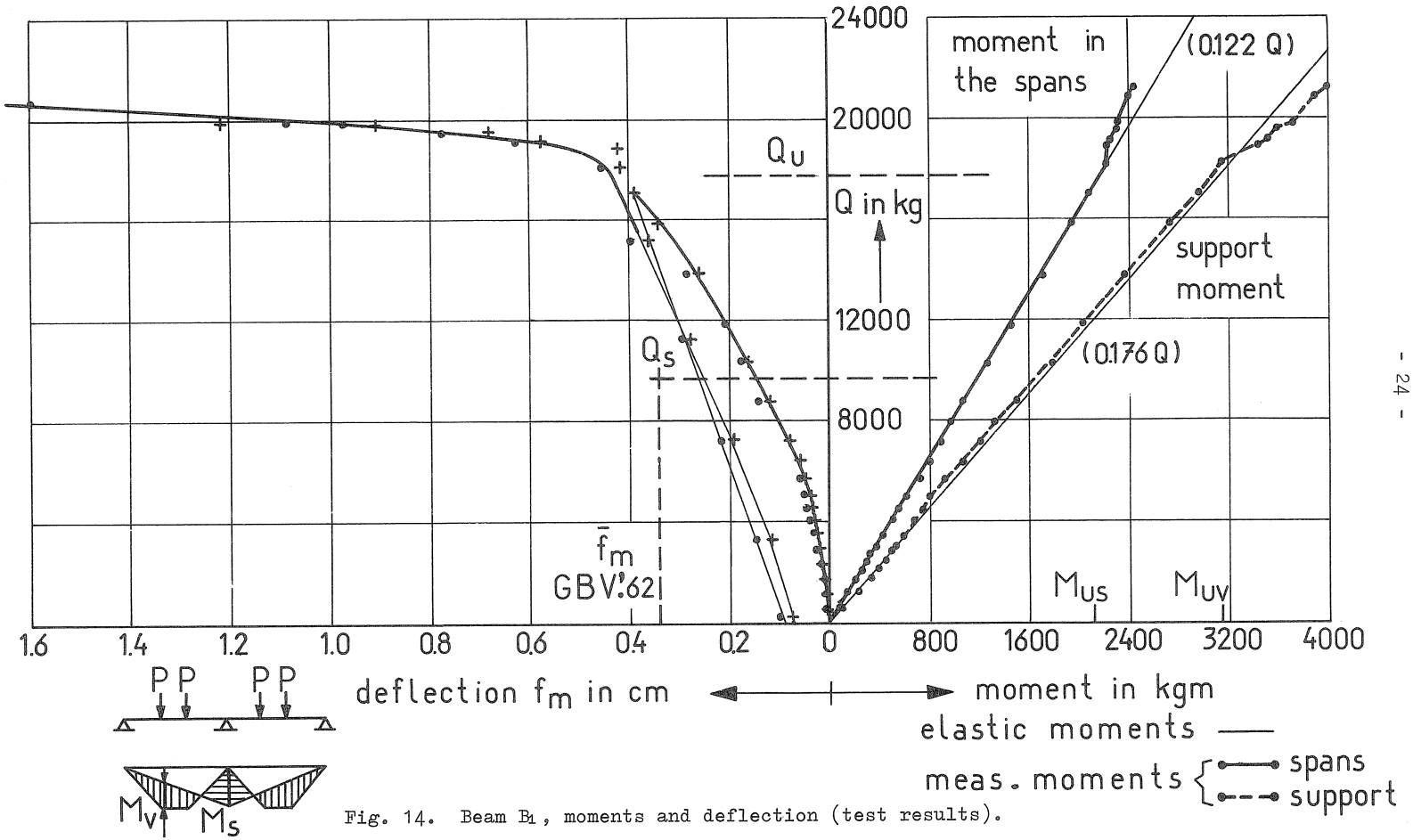

Fig. 14. Beam B_1, moments and deflection (test results).

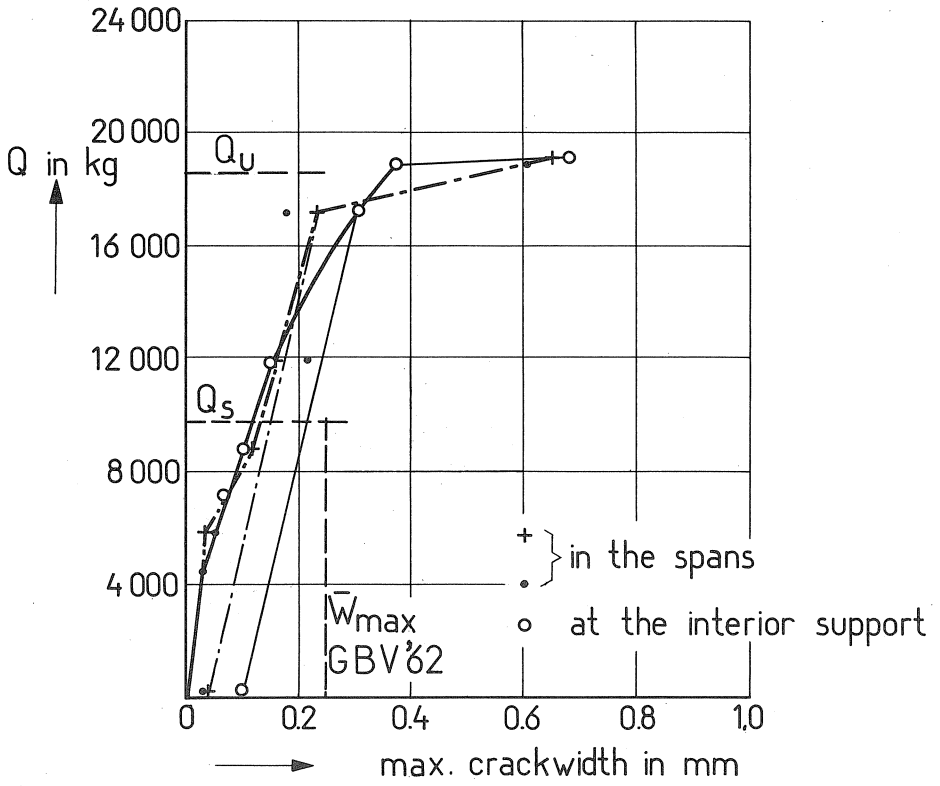

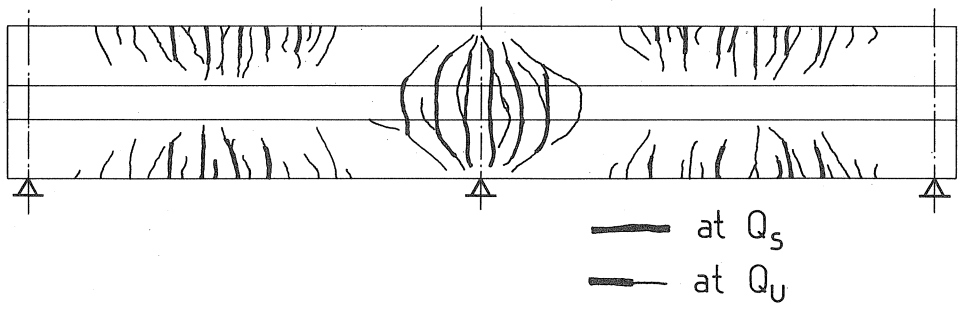

Fig. 15. Beam B_1, max. crackwidth and crackpattern (test results).

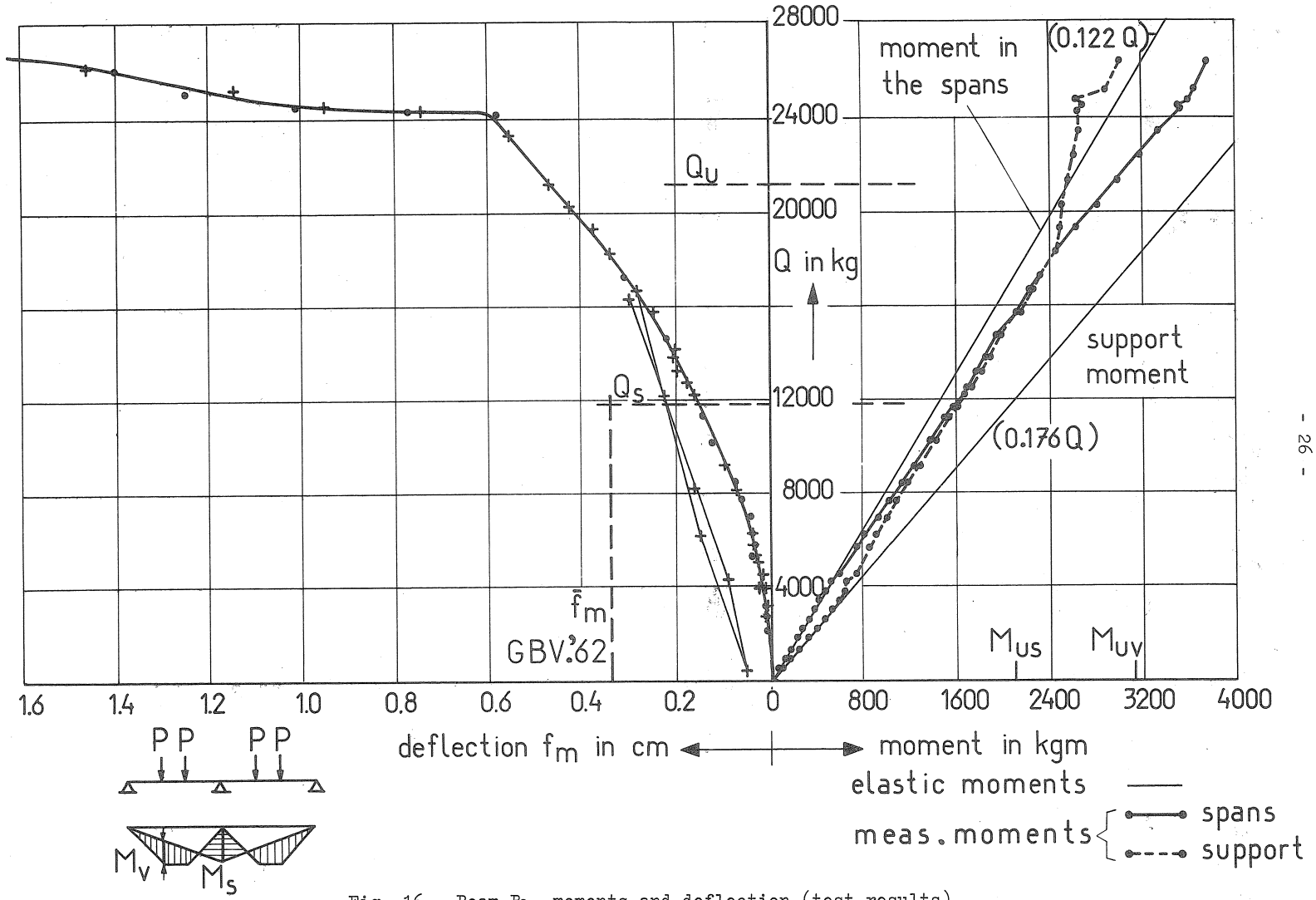

Fig. 16. Beam B_2, moments and deflection (test results).

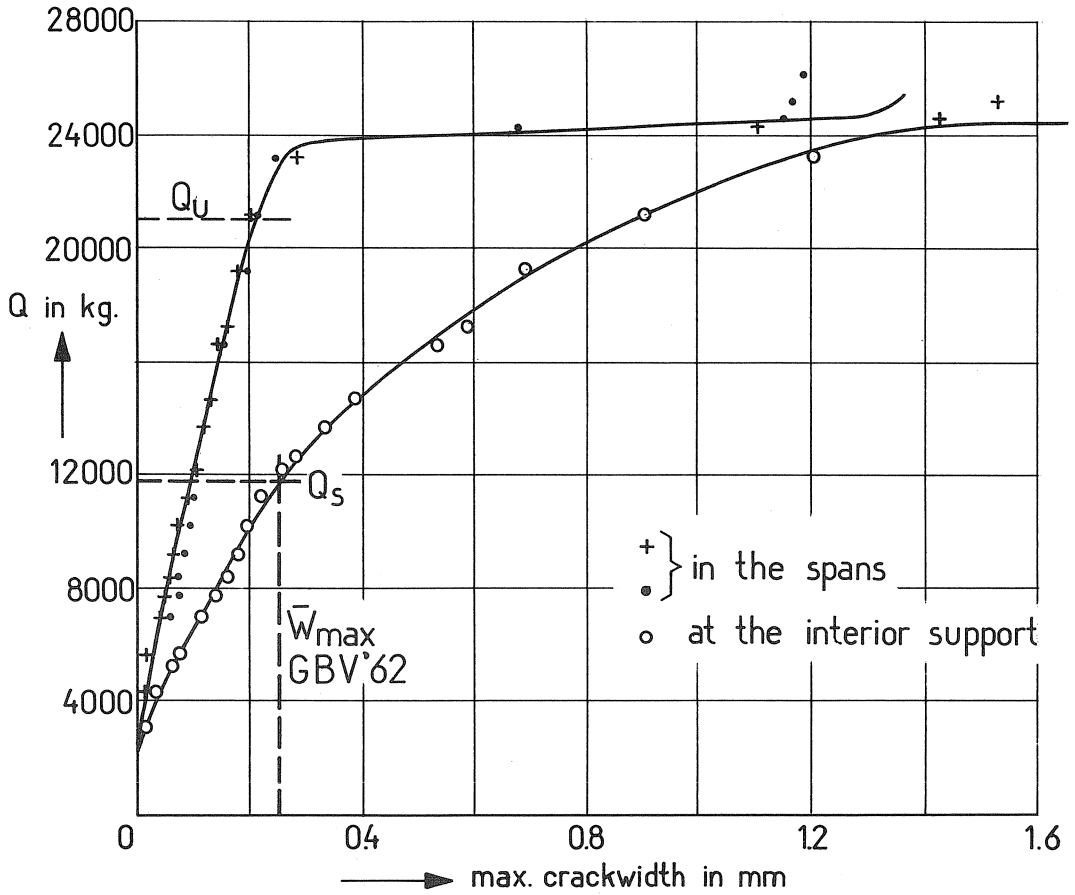

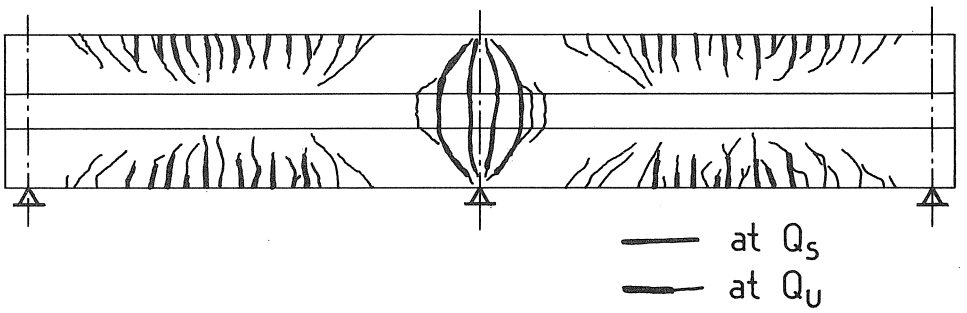

Fig. 17. Beam B_2, max. crackwidth and crackpattern (test results).

- The maximum crack widths in the mid-span regions and over the interior support (these being the regions where positive and negative moments occur respectively) were determined by extrapolation of the strain measured (on a 10 cm gauge length) at the level reinforcement to the extreme tensile fibre. Whenever more than one crack was present within a 10 cm gauge length, the measured strain was distributed over the cracks in proportion to their lengths. Figs. 15, 17, 19 and 21 give the maximum crack widths and the crack patterns of the beams B_1 to B_4.
  In Table 3 it is indicated at what load and which part of the beam a strain corresponding to the yielding of the reinforcement was measured. For comparison, the calculated values already stated in Table 1 have been included in Table 3, as have also the values of the load at which the occurrence of yielding of the reinforcement can be inferred from the moment distribution that was developed.

Figs. 22 and 23 are views of beam B_4 after undergoing the test. Finally, Fig. 24 is a general view of beam B_4 being tested. Also shown in the photograph are the beams B_1, B_2 and B_3 already tested (in the foreground, partly visible, is one of the beams on which the M-$\varkappa$ diagram was measured by means of a four-point loading test).

All the measured curvatures along the lengths of the beams are given in the camparison of the calculated and the measured results, Chapter 4, Figs. 42 to 47.

2.3 Discussion of the results of the measurements

The behaviour of the beams during testing is clearly apparent from Figs. 14, 16, 18 and 20.

In the case of beam B_1 (Fig. 14) the actual distribution of the moments, also in the cracked beam, is found to be in agreement with the calculated elastic values. The calculated collapse load was somewhat exceeded. The bending moment at which the span reinforcement reached the yield stress differs very little from the calculated value. It is particularly notable that in the diagram indicating the actual support moment the yielding of the reinforcement produced no conspicuous point. The reinforcement in question reached the yield stress a fairly short time after

yielding of the mid-span reinforcement occurred, however. Fig. 15 gives the data relating to cracking. In Figs. 14 and 15 the permissible loading is also indicated, this being the calculated collapse load Q_u divided by a factor 1.8. Furthermore the permissible deflection and maximum permissible crack width *) in accordance with the Netherlands code of practice for reinforced concrete (GBV-1962) are indicated in the diagrams concerned. For the beam B_1 under discussion, in which the reinforcement had been installed in conformity with the elastic bending moments, the requirements of the code of practice present no problem at all.

As appears from Fig. 16, in beam B_2 considerable redistribution of the moments occurred after the cracks had formed. Accordingly, in consequence of this redistribution, the yielding of the tensile reinforcement over the support occurred at a substantially higher load than that calculated according to the elastic theory. The bending moment at which yielding of the reinforcement began was in this case also higher than the calculated yield moment for the section concerned. The calculated collapse load was likewise exceeded. As regards deflection, under the permissible loading the beam B_2 was found to remain well below the maximum permissible value. The maximum permissible crack width in accordance with the Netherlands code of practice was just attained under the permissible loading (see Fig. 17). This beam therefore fulfils all requirements, which is a favourable result, considering that in this beam 42% of the support reinforcement was transferred to the mid-span region. **)

In contrast with the above-mentioned beams, beam B_3 does not conform to the requirements of the code as regards the maximum permissible crack width. As Fig. 19 shows, under the permissible loading a maximum crack width (w_{max}) of 0.4 mm was attained. In this beam B_3 50% of the support reinforcement was transferred to the spans. **) There was in fact considerable redistribution of the moments in consequence of cracking, as is apparent from Fig. 18. The deflection under the permissible loading still

---

*) Namely: $\bar{f}_{max} = \frac{1}{500} \quad 0.85 \quad \ell = 0.34$ cm

and $\bar{w}_{max} = 0.25$ mm

**) i.e., of a beam with the same failure load as the beam under consideration.

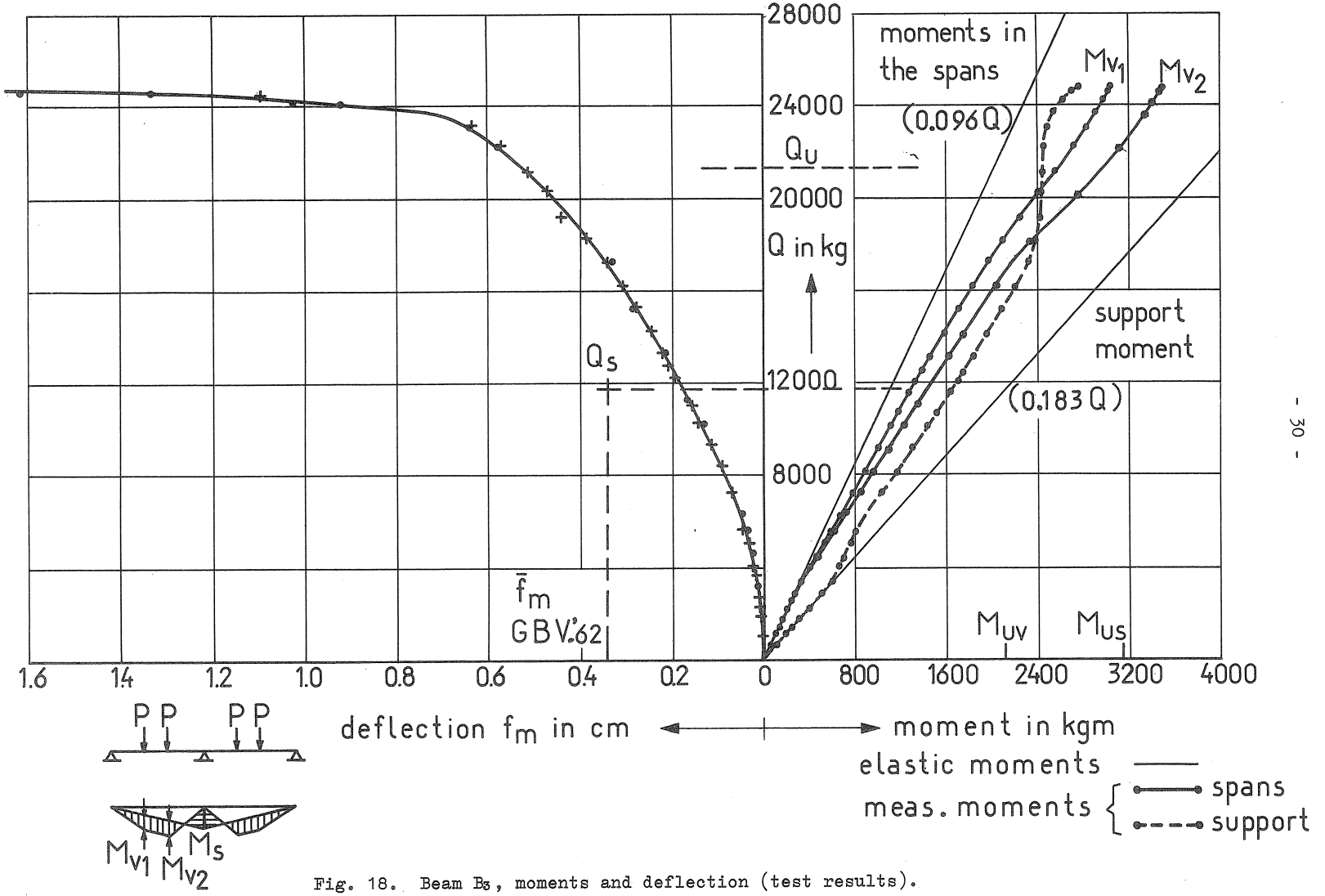

Fig. 18. Beam B_3, moments and deflection (test results).

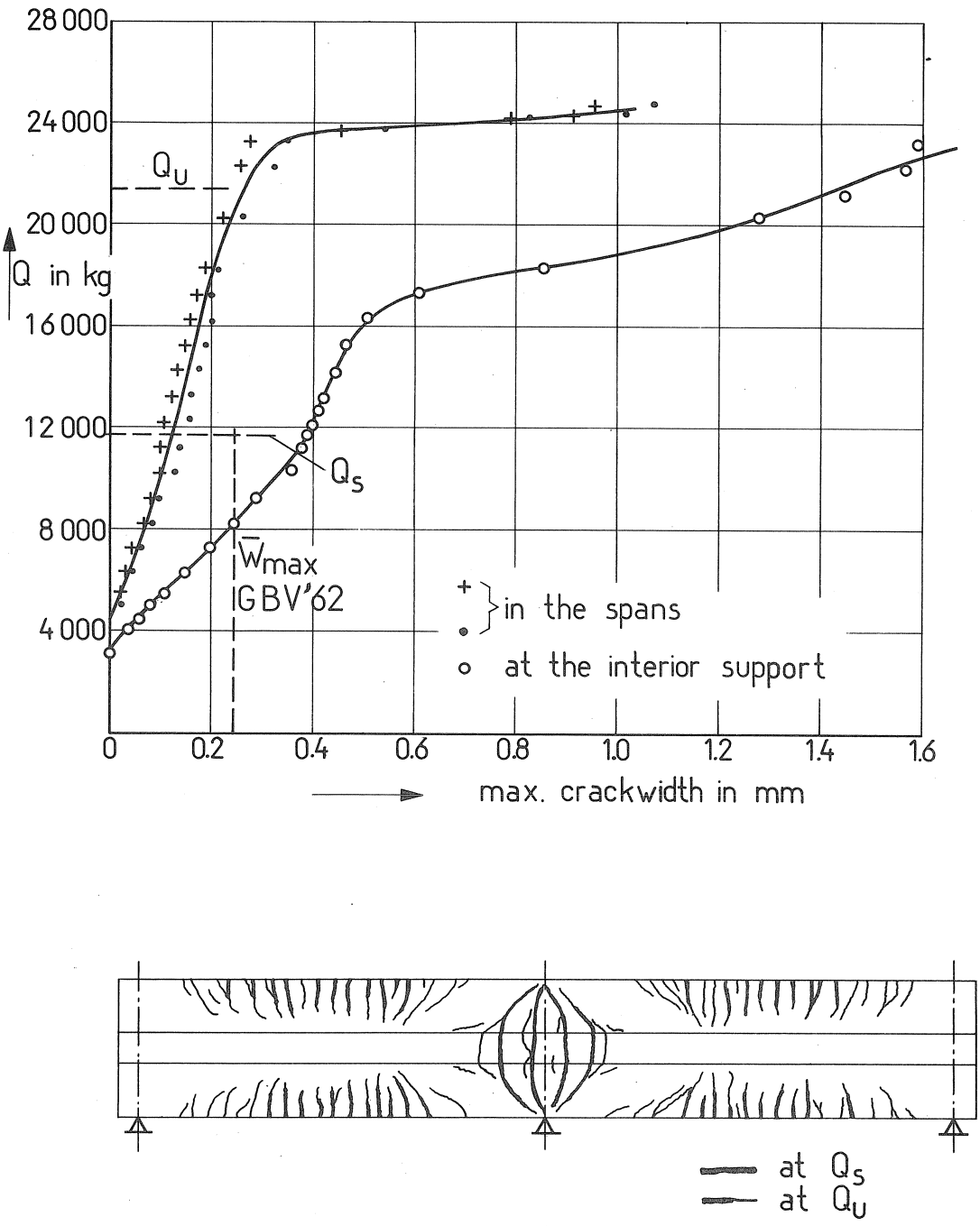

Fig. 19. Beam B_3, max. crackwidth and crackpattern (test results).

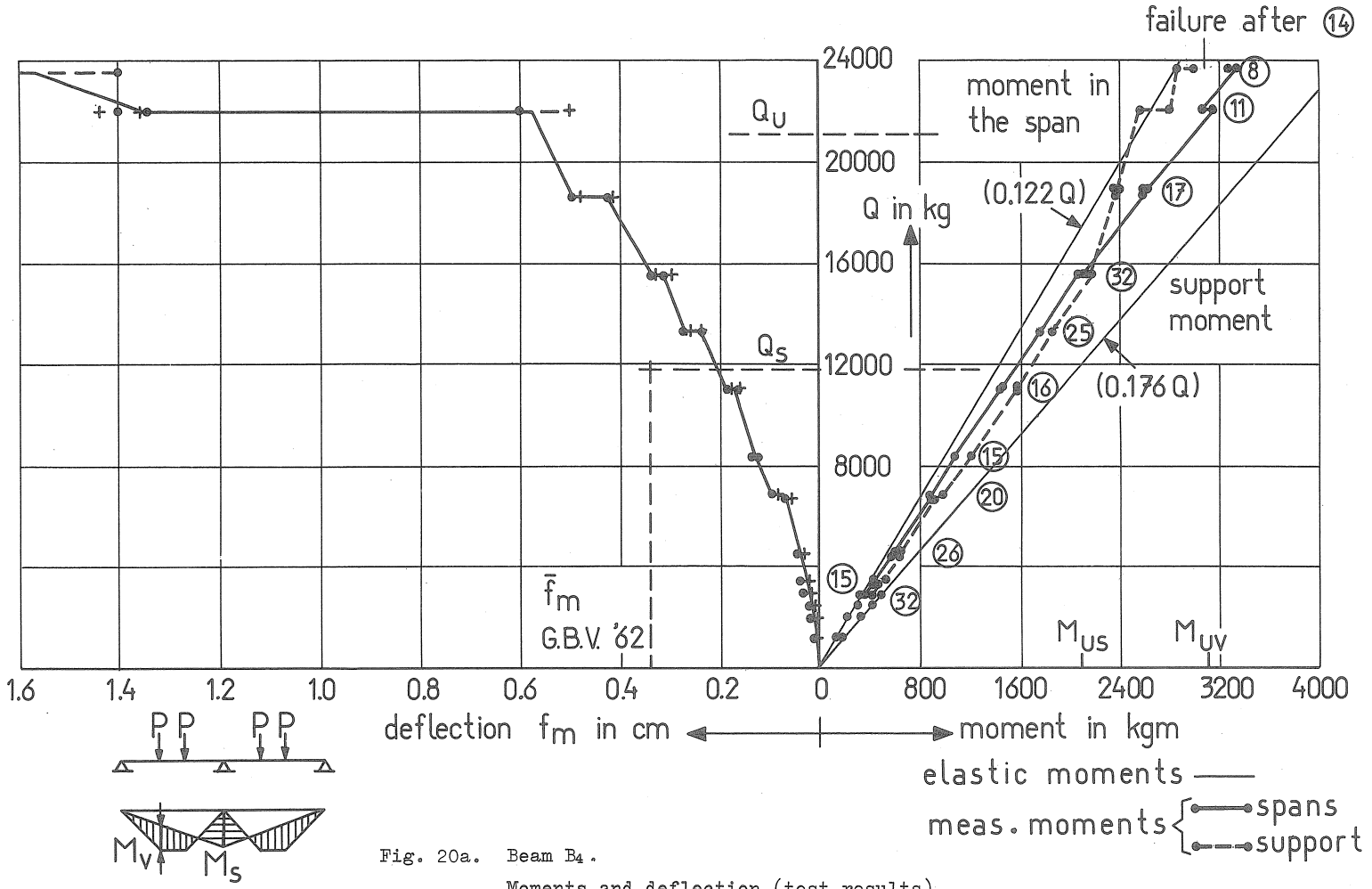

Fig. 20a. Beam B_4.
Moments and deflection (test results).

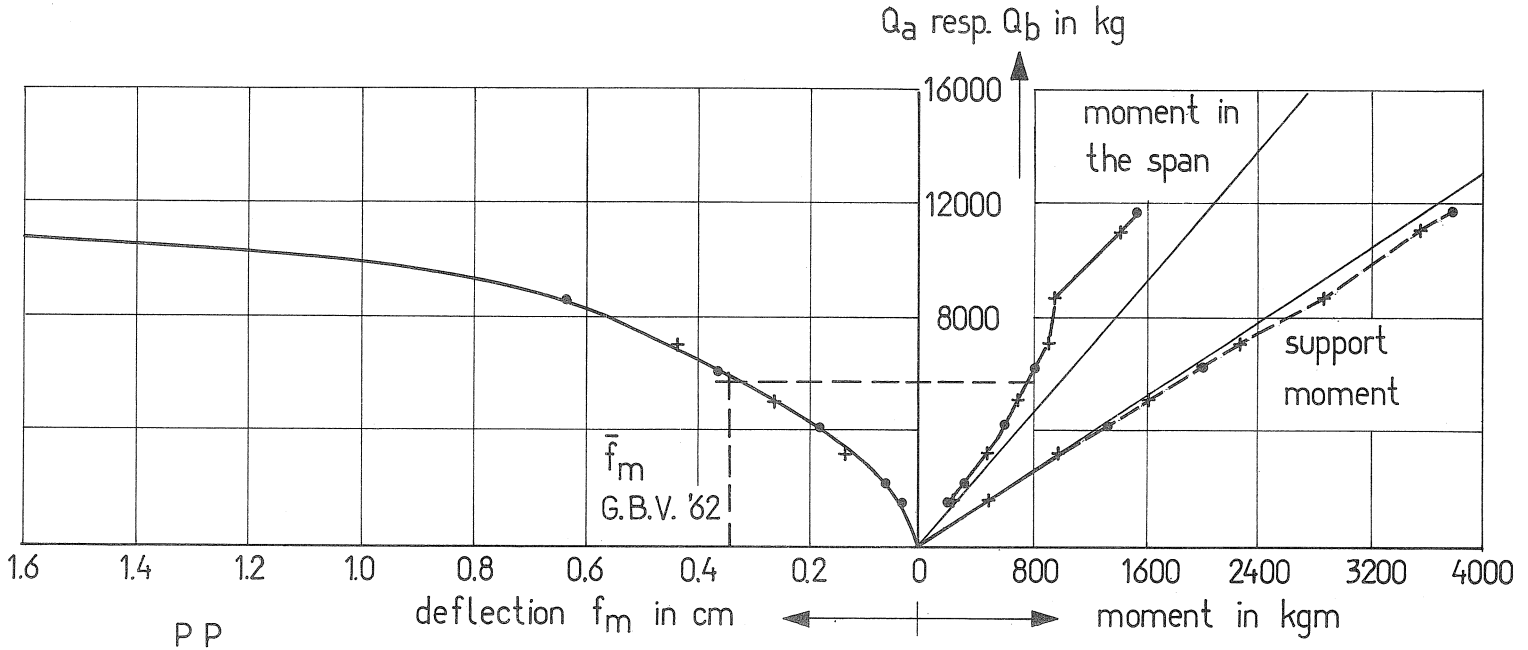

Fig. 20b

Beam B_4.
Moments and deflection.
(test results, one span loaded)

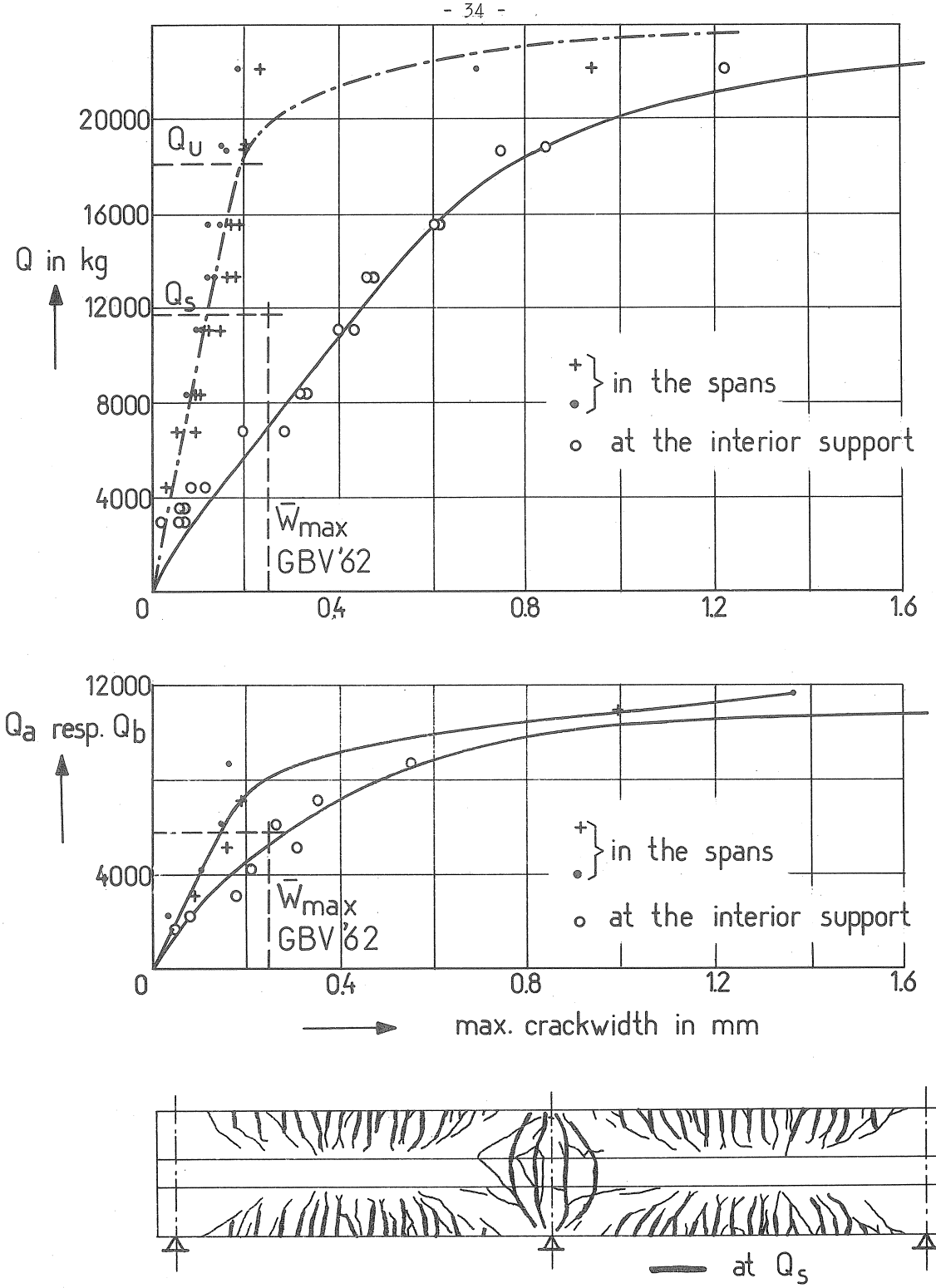

Fig. 21. Beam B_4, max. crackwidth and crackpattern (test results).

conforms to the code requirements, however.

In the case of beam B_4 (see Fig. 20) the moments that occurred were of approximately the same values as those found to occur in beam B_2. Evidently the effect of applying the loading in accordance with the shake-down analysis is of little significance with regard to the moment re-distribution due to cracking. The deflection is thereby substantially increased, although it does not exceed the permissible value under the permissible loading according to the code GBV. The principal difference between the beams B_4 and B_2 is in the greatly increased crack width - due to the load alternations - over the interior support (Fig. 21). In the case of beam B_4 this width is nearly twice as large (namely, $w_{max} = 0.44$ mm) as the maximum crack width measured in beam B_2 under the permissible loading. From Fig. 20 it also appears that, on an average, about 20 of the load repetition cycles described (see also Fig. 11) were needed in order to attain a steady-state condition. The number of cycles necessary to attain a steady-state at each load increment is written in the small circles in Fig. 20. At the last load increment, alternate yielding occurred which, after 14 cycles, resulted in failure. The bending moment at which the tensile reinforcement over the support began to yield is very close to the calculated value of that moment. Because of the fairly considerable redistribution of the moments, yielding of the steel occurs at a higher value of the loading than that calculated according to the elastic theory. The loading at which the beam B_4 failed, in a manner resembling shear failure, after alternate yielding of the reinforcement, was higher than the failure load values calculated for the beams B_2 and B_4. The measured failure load of B_4, however, remained about 10% below the highest value of the loading to which beam B_2 was subjected.

From the values stated in Table 3 there is seen to be some rather substantial difference in the loads at which, according to the measured strains and the measured distribution of the moments, yielding of the tensile reinforcement over the central support must have taken place. The most probable cause of the difference must simply be sought in the fact that, in the circumstances, the strain measured on a gauge length of 10 cm is not a reliable criterion for the average steel strain over that distance. Shear-like effects and bond slip play an important part in this context.

Table 3. Sequence of appearance of the plastic hinges

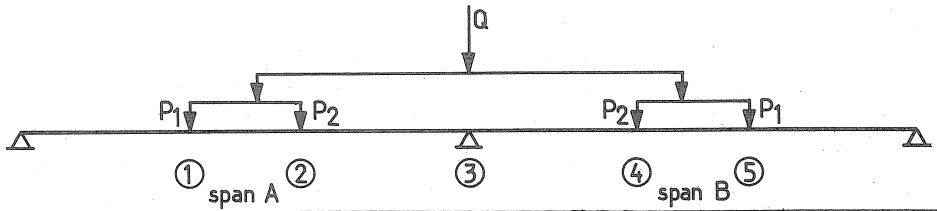

sequence of appearance		1st plastic hinge at	2nd	3rd	4th	5th	explanation
B1	1) Q_1	18000	18000	19000	at 2 and 4 no yielding		1) Q_1 = the load at which the plastic hinge appeared according to the measured moments
	2) Q_2	⑤ 17519	① 17519	③ 17634			
	3) Q_3	15859 (4-5)	17181 (4-5)	17181 (17-18)			
B2	1) Q_1	18000	24600	24600			2) Q_2 = theoretical load for the appearance of the plastic hinge concerned (see Table 2)
	2) Q_2	③ 11978	① 21076	⑤ 21076	④	② no yielding	
	3) Q_3	12196 (16-17)	16650 (4-5)	17230 (3-4)	23267 (9-10)		
B3	1) Q_1	18000	23800	23800	23800	23800	3) Q_3 = load at which the yield strain of the reinforcement was measured. The measuring points are given between brackets (gauge length 10 cm, see Fig. 13).
	2) Q_2	③ 11522	④ 21291	⑤ 21291	① 21291	② 21291	
	3) Q_3	8270 (17-18)	18258 (11-12)	18258 (4-5)	19660 (5-6)	20243 (8-9)	
B4	1) Q_1	16000	23500	23500			
	2) Q_2	③ 11978	① 21076	⑤ 21076	②	④	
	3) Q_3	6806 (17-18)	$\frac{1}{2}Q$ = 7014 (4-5) span A loaded	18649 (5-6)	18649 (7-8)	18700 (8-9)	

Values of Q in kg.

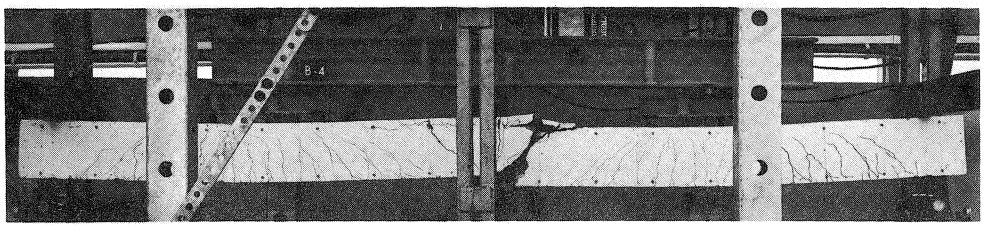

Fig. 22. Beam B_4 after failure.

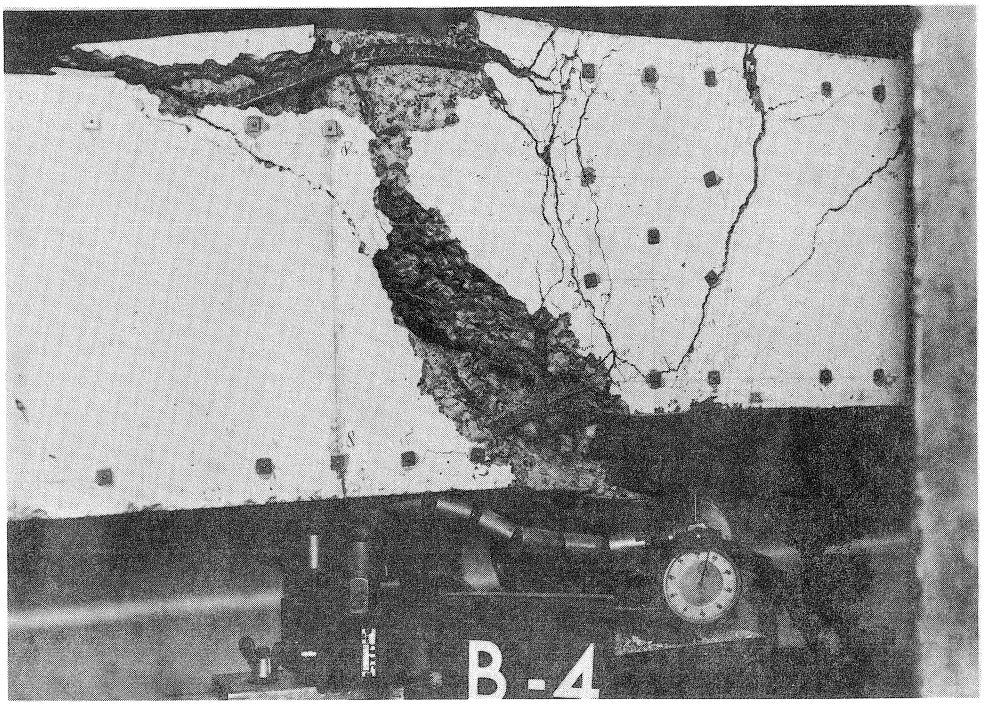

Fig. 23. Interior support section of beam B_4 after failure.

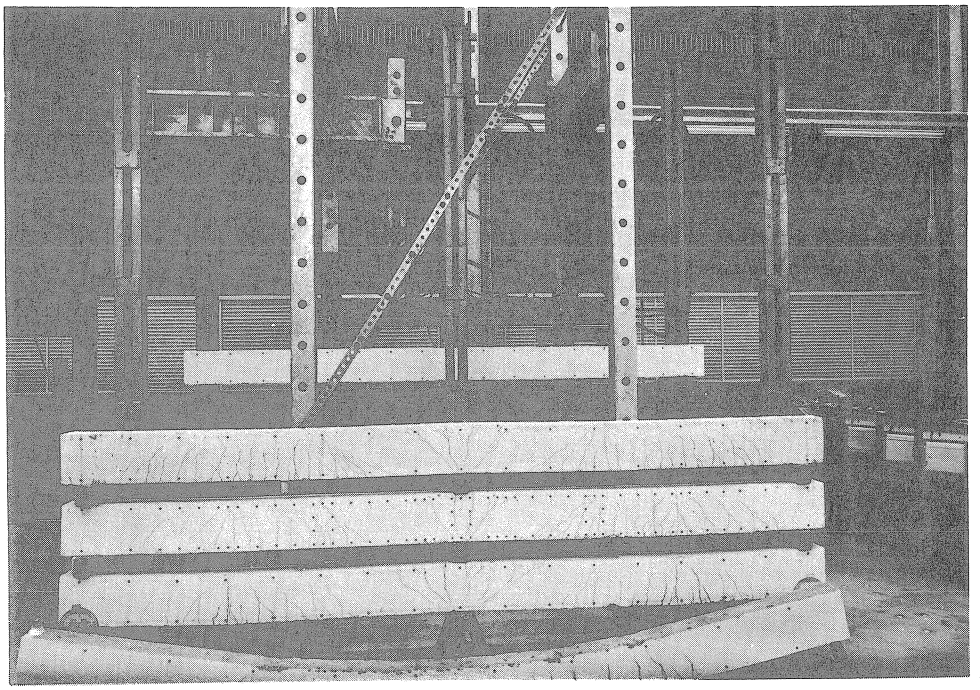

Fig. 24.

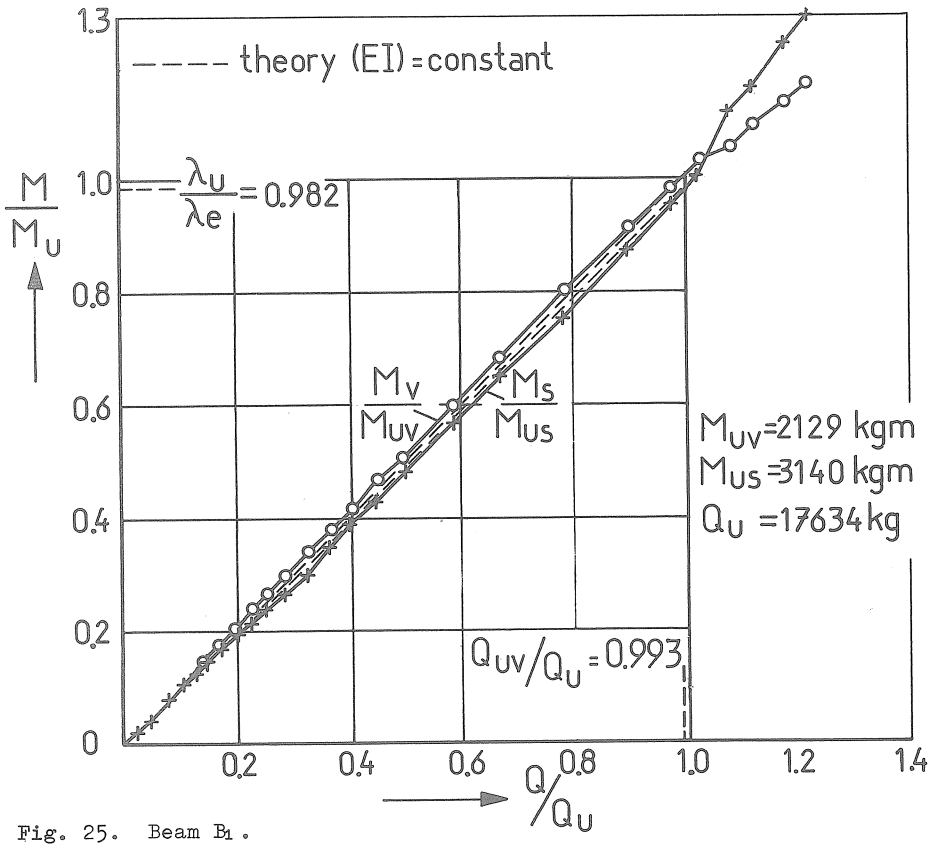

Fig. 25. Beam B_1.

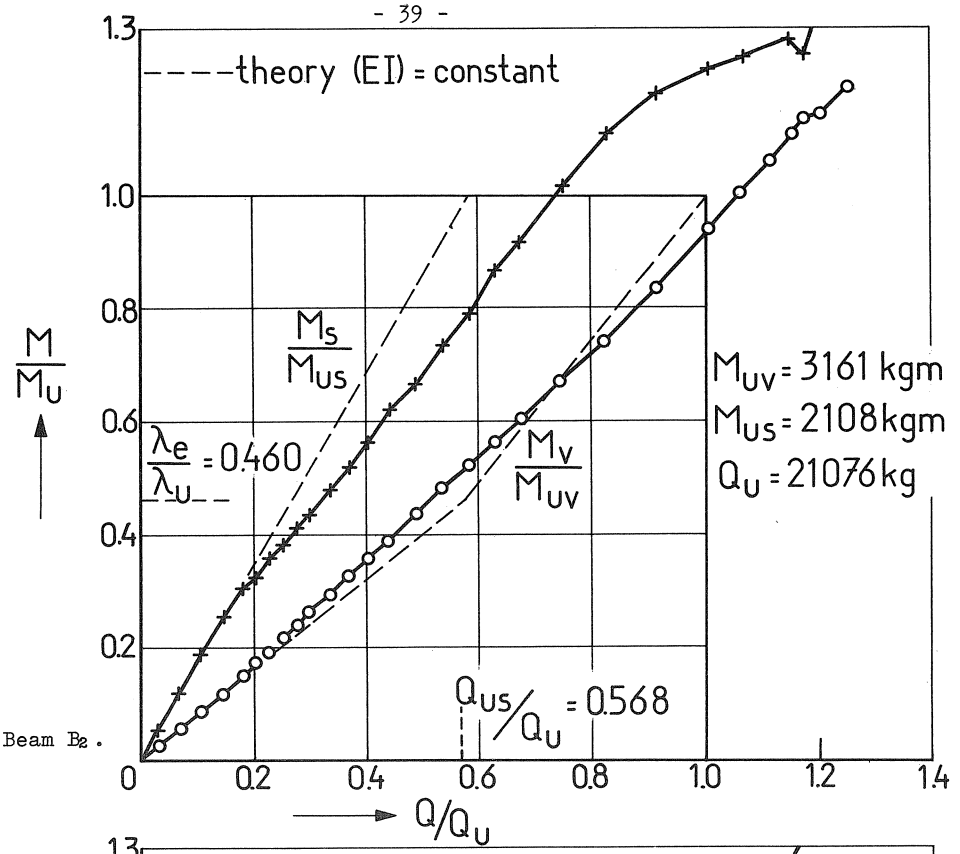

Fig. 26. Beam B_2.

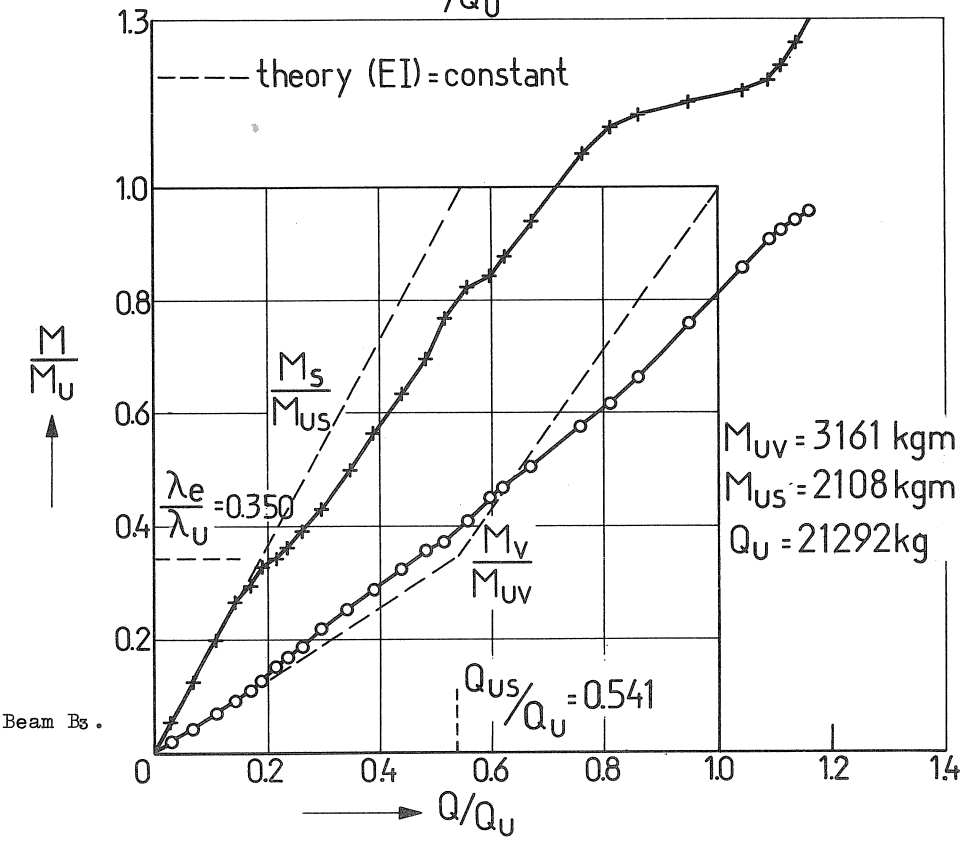

Fig. 27. Beam B_3.

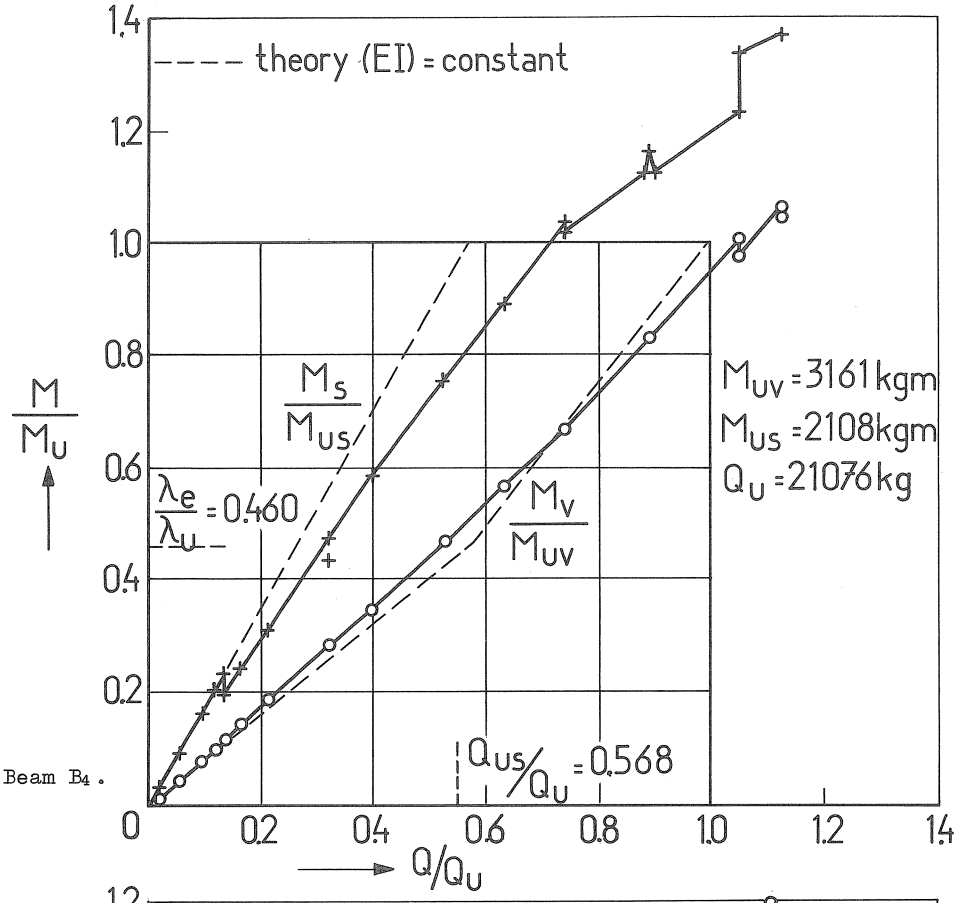

Fig. 28. Beam B_4.

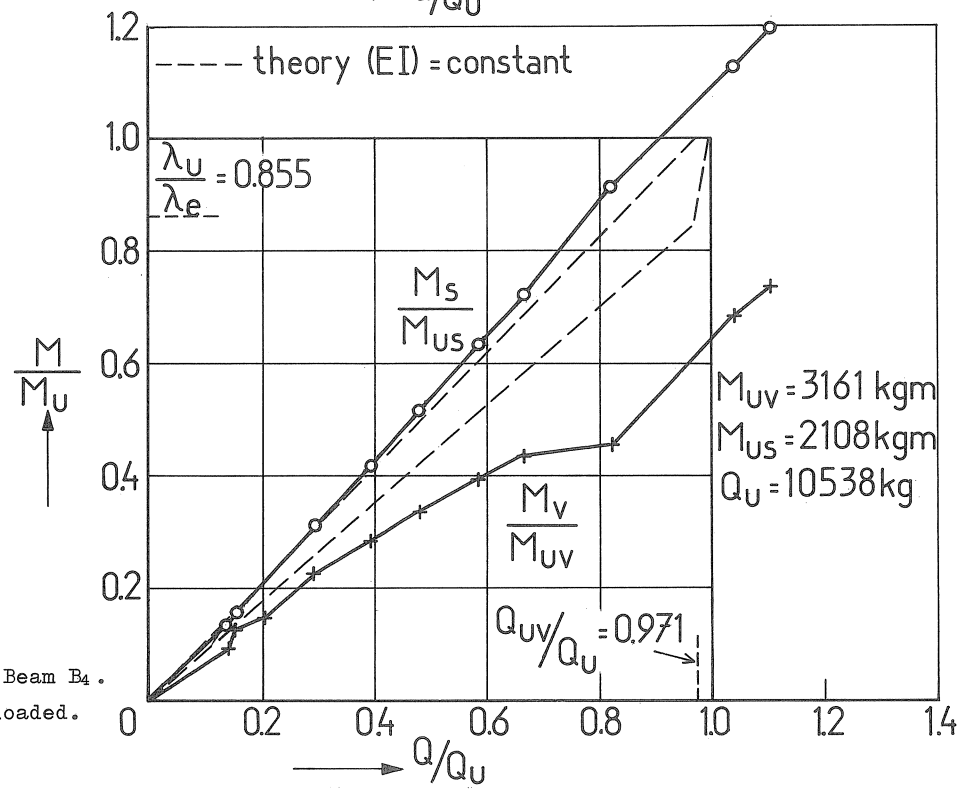

Fig. 29. Beam B_4.
One span loaded.

2.4 Conclusions from the tests

The following conclusions can be drawn from the experimental investigation, within the scope of the research-work performed here:

(a) If the quantities of reinforcement in a continuous beam are adapted to the magnitude of the elastic moments, then the actual distribution of the bending moments will be as in a homogeneous elastic beam.

(b) With the above-mentioned method of reinforcement of the beam under consideration it is possible amply to fulfil the requirements of the Netherlands code of practice with regard to deflection and maximum crack width.

(c) As a result of transferring reinforcement from the central support to the spans there occurs a redistribution of the moments in consequence of cracking. The actual support moment decreases and the actual span moments increase in relation to the respective values calculated according to the elastic theory.

(d) If 40% of the support reinforcement is transferred to the mid-span regions, then the largest measured crack width of 0.25 mm will still fulfil the requirements laid down in the Netherlands code of practice.

(e) As a result of alternate loading of a continuous beam the crack width in the region where reinforcement has been removed is greatly increased.

(f) The load alternations have little effect on the redistribution of the moments.

(g) With such loading in accordance with the shake-down analysis it was found that, as a result of alternate yielding, the rotational capacity of the first plastic hinge formed was reached sooner, with the result that the collapse load was lower (but not below the theoretical failure load).

2.5 Extra investigation

Tests were carried out, as preliminary research, to determine the M-$\varkappa$ diagrams of the sections of the B-beams, discussed before.
The purpose of this was to be able to find the best interpretation for the experimental results of the continuous B-beams.

The beams concerned were tested according to the well-known 4-point loading test. The cross-section, the steel - and concrete properties were of course the same as they were for the continuous beams.
Figs. 30 and 31 show the measured M-$\varkappa$ diagrams, while Fig. 32 gives a

survey of one of the test beams after yielding.

The measured M-$\varkappa$ diagrams were in good agreement with the results of other tests concerning the moment-curvature relation of reinforced concrete.

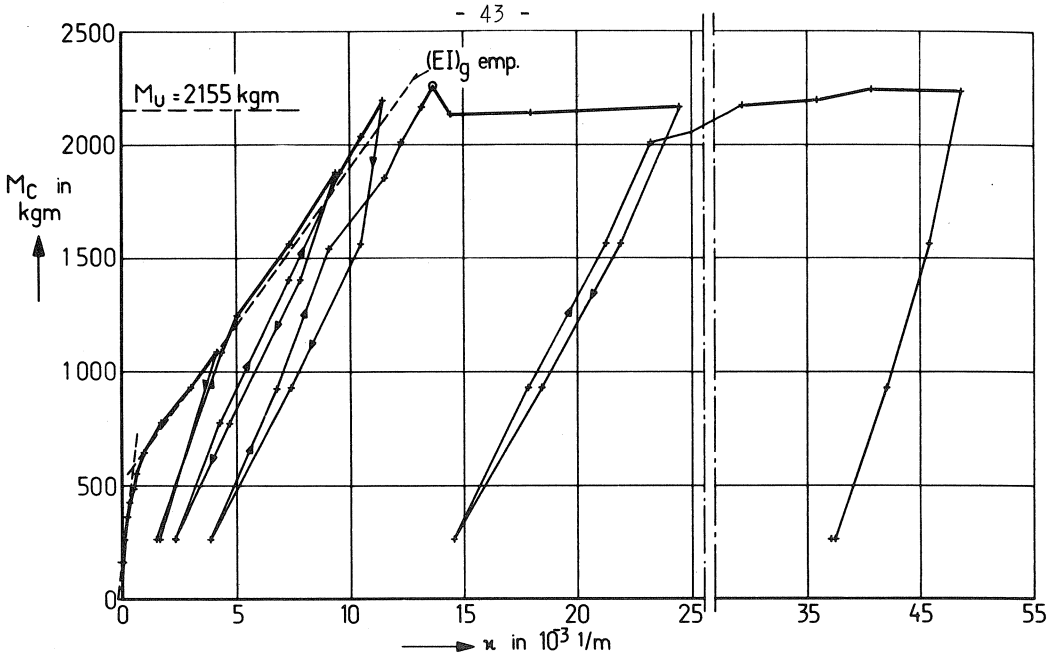

Fig. 30 Beam A_1
(ω_0 = 0.64%, ω_0' = 0.96%)

+ measured values
o yieldpoint. only the load was measured

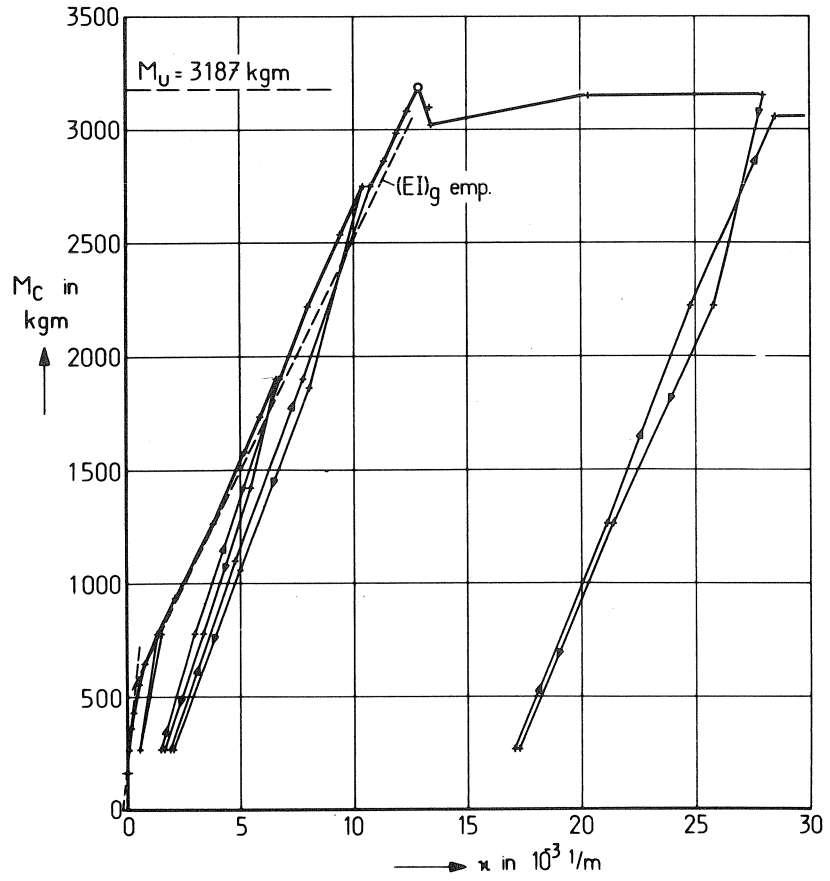

Fig. 31 Beam A_2
(ω_0 = 0.96%,
ω_0' = 0.64%)

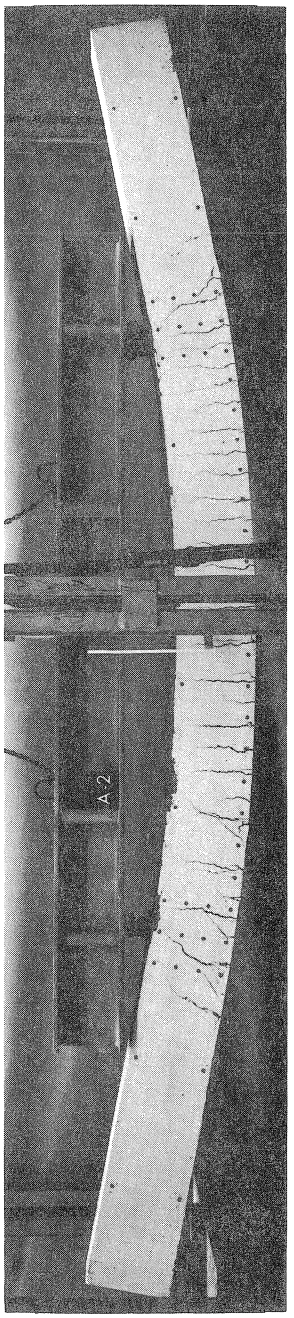

Fig. 32 Beam A_2 after yielding

3. The analysis of statically indeterminate reinforced concrete structures

As has been explained in the introduction, an analysis procedure has been programmed with the object of, as it were, being able to carry out model research with the aid of the computer. It is in fact essential to be able to calculate the actual moment distribution, the deflection and the crack widths satisfactorily. In this approach to the problem it is of course necessary, among other things, to enable the change in bending stiffness, for instance when the concrete cracks, to be taken into account in the calculation. This chapter describes the analysis procedure that has been programmed.

The programme is suitable for the analysis of plane structures consisting of bar-type members which are not affected by stability problems The second-order effects are not taken into account in the calculations. Besides the analysis of the force distribution and deformations due to a once-only load increasing from zero to collapse load (using a M-$\varkappa$ diagram as drawn in Fig. 33), the effect of load alternations can also be determined by means of the available programme. For that purpose the M-$\varkappa$ diagram as represented in Fig. 34 is utilised.*) Calculations in accordance with shake-down analysis are therefore also possible. Furthermore, applied deformations as well as loads can be introduced into the calculations.

3.1 Describtion of the calculation procedure

For the purpose of carrying out the analysis the structure to be analysed is subdivided into beam elements by means of joints (nodes). Two adjacent joints should be chosen so close together that, relating to an element's stiffness with regard to a load, the average moment of the element in question can be adopted. In calculations carried out so far the length of the elements were about equal to the depth of the beam concerned.

The loading is applied in the form of centrated forces at the joints.

For the time being shear force effects will be neglected. The calculation procedure is therefore as follows.

---

*) The latter is discussed in a separate paper: The moment-curvature relation of reinforced concrete; Heron, vol. 17 (1970), no. 2.

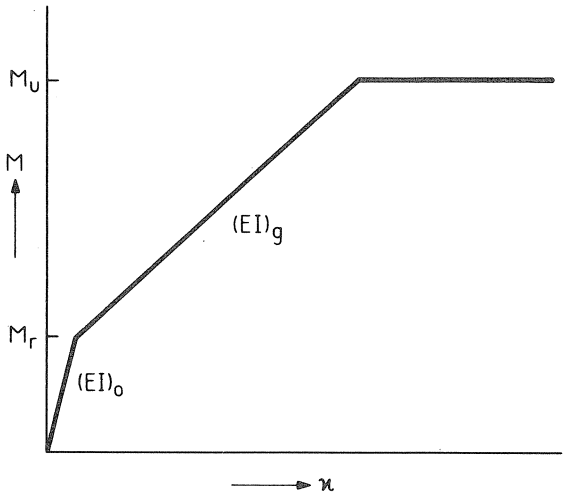

Fig. 33 M-$\varkappa$ diagram for a first-time loading

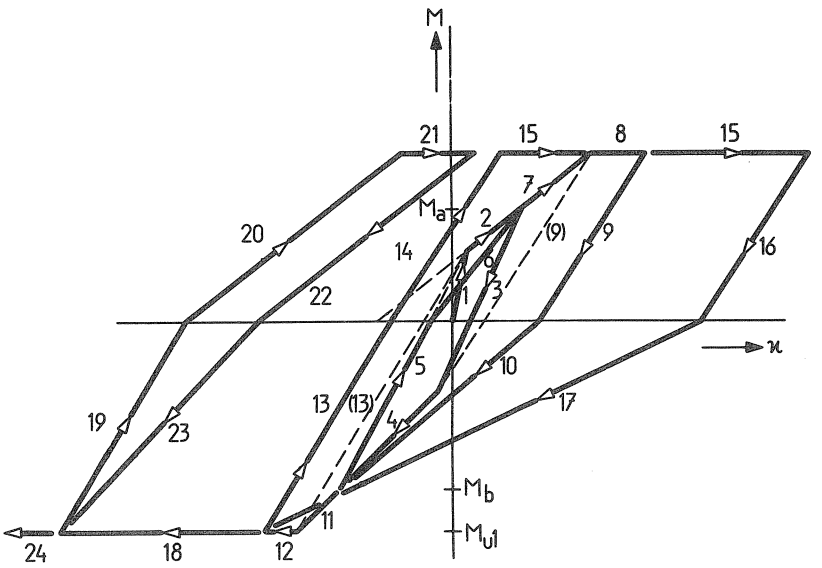

Fig. 34 Schematised M-$\varkappa$ diagram in the case where the moment changes its sign

A load which is larger than the estimated failure load is applied to the structure. At this stage of the analysis no cracking has as yet occurred anywhere in the structure. In all its elements the flexural stiffness is $(EI)_o$, corresponding to the first branch of the M-$\varkappa$ diagram for reinforced concrete (see Fig. 33). It is now calculated (with a normal, linear calculation) at what percentage of the applied loading the average moment in one of the beam elements is the first to attain the cracking moment M_r. At that loading Δp_1 are calculated: the moments at the ends of the elements $\Delta M_{i,1}$, the deflections $\Delta f_{i,1}$ at the joints (nodes) and the average curvature $\Delta \varkappa_{i,1}$ in the elements. The relevant, cracked element of the structure has from now on the bending stiffness $(EI)_g$, corresponding to the second branch of the M-$\varkappa$ diagram. Then the full loading is again applied, to this structure in which the one 'exceptional' beam element has the stiffness $(EI)_g$ and the others have the stiffness $(EI)_o$. It is now investigated at which percentage Δp_2 of the total loading the moment of the subsequent element reaches its limit-moment now valid, i.e., $M_r - \Delta M_{i,1}$, or should that occur earlier, until the limiting 'yield' moment $M_u - \Delta M_{i,1}$ develops in that element for which the stiffness is $(EI)_g$. The total moments $\Delta M_{i,1} + \Delta M_{i,2}$ and deformations $\Delta f_{i,1} + \Delta f_{i,2}$, etc., associated with the load $\Delta p_1 + \Delta p_2$ now acting upon the structure are then calculated.

The calculations are continued in this way. In the element where the average moment attains the cracking moment, the stiffness is in each case altered from $(EI)_o$ to $(EI)_g$ (in general the limit moment then valid = $M_r - \sum_{j=1}^{n} \Delta M_{i,j}$). The magnitude of the load increments depends on whether the stiffness has to be modified somewhere; in general, the increments are not equal. If the yield moment develops at any particular point, a complete hinge is applied at the joint concerned. The calculation is stopped when a collapse mechanism develops in the structure.

As shown the limit-values for the moments, at which the flexural stiffness of the elements has to be changed, are each time corrected because of the moments that occur with regard to foregoing load increments. This is simply the consequence of the fact that the calculations for each load increment are applied for a new, unloaded structure which has some changed stiffness properties with regard to the last one. The results obtained for each load increment can then be added together to determine the actual moments etc. in a certain stage of loading of the structure.

In the computer programme the calculation is therefore performed linearly in steps. This procedure is not an iteration method, since only one linear calculation is performed for each load increment. The linear calculations for each load interval, are carried out in accordance with the displacement method, in which the displacement components of the joints (nodes) between the beam elements are therefore the unknowns in a set of equations.

Since the M-$\varkappa$ diagram of reinforced concrete can be approximated quite well by (three) straight lines, this calculation procedure is, in principle, virtually an "exact" one. With the programme a non-linear behaviour pattern can, however, also be fairly closely approximated. For example, a curved M-$\varkappa$ diagram can, after all, be represented by a larger number of short straight portions.

From a comparison between the calculated results and the measured results, which will be discussed in chapter 4, it was concluded that the shear deformation of the cracked parts of the beams had wrongly been neglected. From that moment on, the effect of this was therefore taken into account. On the one hand this is done in the form of a correction applied to the bending stiffness adopted to the M-$\varkappa$ diagram measured in a region of constant moment. On the other hand a correction is applied to the calculated deflection.

In the case where the shear force effect is taken into account the calculation procedure is in fact the same as discussed before.

With regard to the subdivision of the structure also the same rules were followed as given earlier. Normally in this cases, however, the elements which are directly beside an interior support, or elsewhere in parts where the shear force excercises relatively the greatest effect, are in turn divided into two equal parts.

The flexural stiffness is directly corrected for shear effect in accordance with the rules discussed in the next part of this chapter (3.2.2). The correction factor concerned appears to be dependent of the actual shear force/moment ratio in the cracked member. Therefore, that ratio must be estimated. Before accepting the calculated moment distribution as correct, it is first investigated what the stiffness would have to be for the shear force/moment ratio occurring in the cracked element. If this value differs more than 5% from the bending stiffness introduced

into the calculation, then the new stiffness value is introduced, and the calculation of moments is carried out again. On the other hand, if it differs by less than 5%, then it is investigated in accordance with the normal calculation procedure, at what loading in the next element the average moment becomes equal to the cracking moment etc.

The deflection calculated from the moment distribution is likewise corrected for the effect of shear force; the magnitude of this effect is determined by means of a calculation as set forth in Fig. 35. In the condition shown in that diagram all but two of the members have cracked.

The deflection Δf_t due to shear force thus calculated is (for each joint) added to the deflection f of the joint in question, calculated from the moment distribution. The total value $f + \Delta f_t$ is introduced as the deflection at the points concerned.

The flow diagram of the computer programme is given on page 51.

3.2 Incorporation of the reinforced concrete properties

For the sake of completeness it will first be explained how the flexural stiffness of reinforced concrete is incorporated into the computer programme.

Furthermore, it will be described which shear stiffness is taken into account and how the correction of the shear-effect is developed with regard to the flexural stiffness.

Finally, the manner in which the maximum crack width is calculated will be established also.

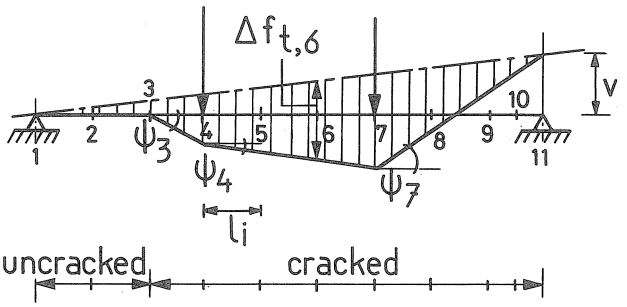

$$\psi = \frac{T}{(GB)_g} \text{ ; relative deflection of the joints : } \psi_i . l_i = \frac{T . l_i}{(GB)_g}$$

$$v = \sum_{i=1}^{10} (\psi_i \cdot l_i)$$

$$\Delta f_{t,6} = \sum_{i=1}^{5} (\psi_i \cdot l_i) + \frac{5}{9} v$$

Fig. 35. Calculation of the additional deflection due to shear.

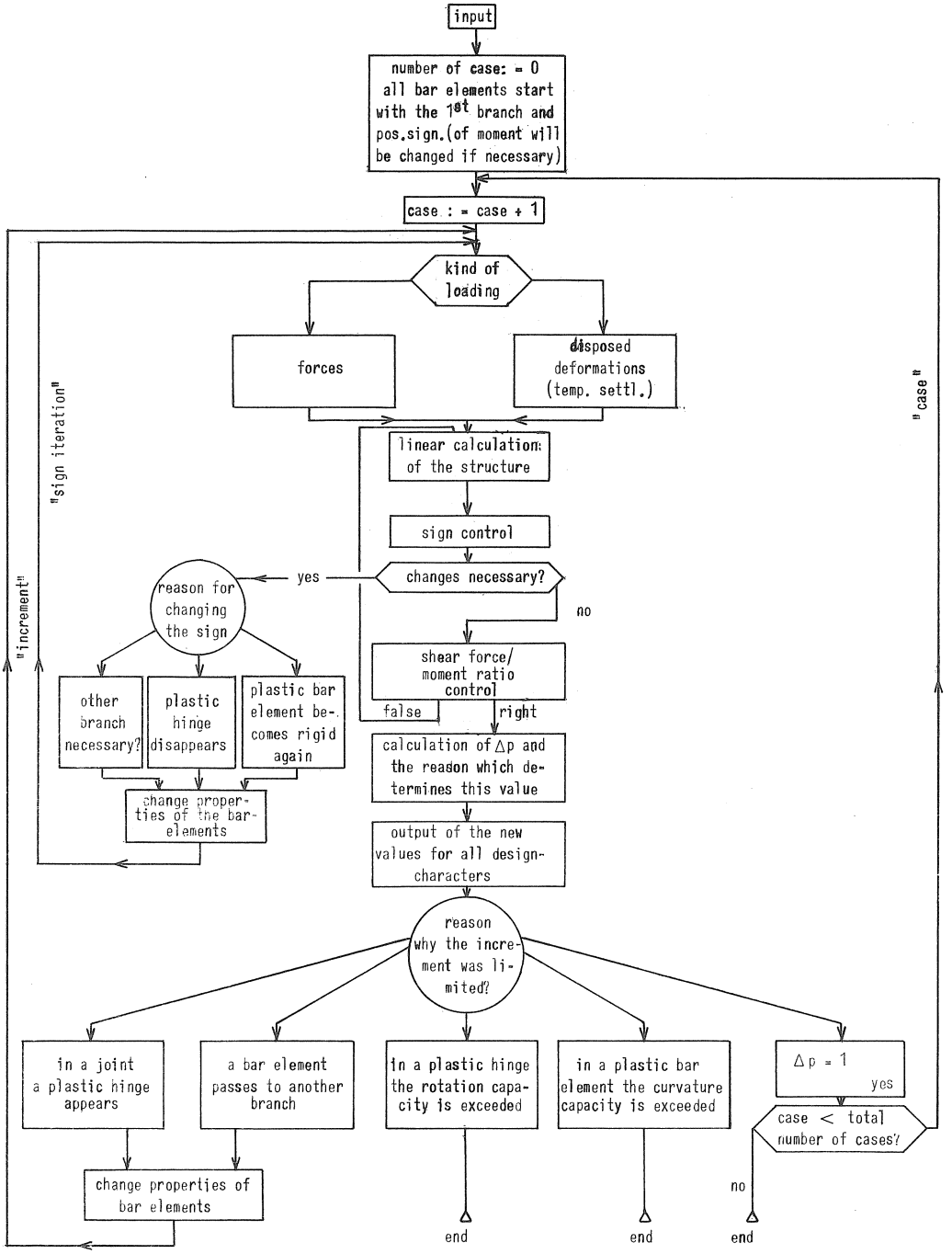
input
number of case: = 0
all bar elements start with the 1st branch and pos.sign.(of moment will be changed if necessary)
case : = case + 1
kind of loading
forces
disposed deformations (temp. settl.)
linear calculation of the structure
sign control
changes necessary?
yes
no
reason for changing the sign
other branch necessary?
plastic hinge disappears
plastic bar element becomes rigid again
change properties of the bar-elements
shear force/ moment ratio control
false
right
calculation of Δp and the reason which determines this value
output of the new values for all design-characters
reason why the increment was limited?
in a joint a plastic hinge appears
a bar element passes to another branch
in a plastic hinge the rotation capacity is exceeded
in a plastic bar element the curvature capacity is exceeded
Δp = 1
yes
case < total number of cases?
no
change properties of bar elements
end
end
end
"sign iteration"
"increment"
"case"

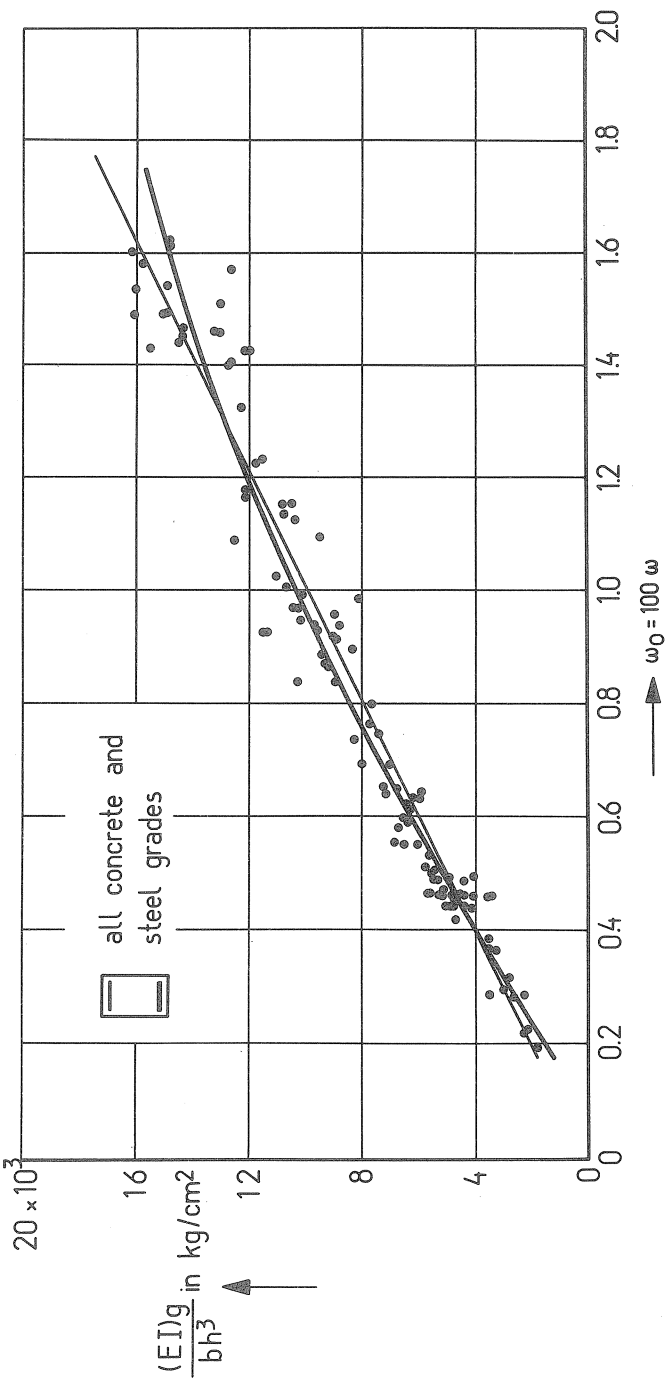

Fig. 36
The bending stiffness $(EI)_g$ of the cracked state as a function of the percentage of tensile reinforcement.

3.2.1 The M-$\varkappa$ diagram of reinforced concrete

As mentioned before this diagram can be approximated by straight lines as represented in Fig. 33.

Prior to the occurrence of cracking, the bending stiffness is

$$(EI)_o = E'_{bo} \cdot I_{bo},$$

where

E'_{bo} = modulus of elasticity of concrete (tangent in the origin of the stress-strain diagrams), which can be found from the cube strength as $E'_{bo} = (\frac{1}{3}\sigma'_w + 200) \quad 10^3$ kg/cm^2;

I_{bo} = moment of inertia of the section including the reinforcement.

When the cracking moment M_r is reached, the stiffness changes. The cracking moment is approximately determined by

$$M_r = \sigma_b \cdot W_{bo},$$

where

σ_b = tensile strength of the concrete and can be taken as $\sigma_b = 1.2\ (\frac{1}{20}\sigma'_w + 10)$ kg/cm^2;

W_{bo} = section modulus, the reinforcement included.

The results obtained from the above mentioned formulas appear to be in good agreement with reality.

For the stiffness $(EI)_g$ in the cracked state the following empirical expression has been deduced for normal cases:

$$(EI)_g = (-2.5\,\omega_o^2 + 13.9\,\omega_o - 1.1)\ bh^3 \quad 10^3 \text{ kgcm}^2$$

where ω_o is the percentage of tensile reinforcement, b is the width, and h is the effective depth of the section. The above relation between $(EI)_g$ and ω_o is represented by the thickly drawn curve in Fig. 36. The points plotted in that diagram are the measured values. In the computation programme the bending stiffness is calculated with this formula. (The given curve can be approximated by a straight line for which $(EI)_g = \omega_o \cdot bh^3 \quad 10^4$ kgcm^2 $= 0.48\ E_a \omega\ .bh^3$ kgcm^2; this line is drawn thin in Fig. 36.)

The horizontal third branch of the M-$\varkappa$ diagram occurs at the yield moment. This moment is found to be in reasonable good agreement with the failure moment calculated according to the ultimate-load method, see Appendix II. The analysis is accordingly based on a parabolic stress-

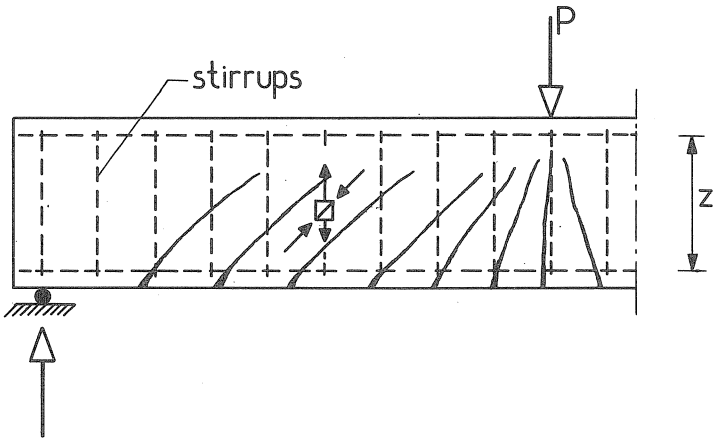

Fig. 37. Shear force region.

strain diagram for concrete with:

- extreme concrete stress $\sigma'_{bu} = 0.6\ \sigma'_w$;
- strain of concrete at failure $\varepsilon'_{bu} = 3.5‰$, as laid down in the Netherlands code of practice (GBV '62)

Some M-$\varkappa$ diagrams for various reinforcement percentages were already presented in Fig. 2 by way of illustration.

3.2.2 Effect of shear force

The shear strain of uncracked concrete is taken as equal to that of a homogeneous elastic material and is given by the well-known formula:

$$\psi = \frac{T}{G.B}$$

where ψ is the shearing strain (angular displacement due to shear force), T is the shear force, and G is the shear modulus (or modulus of rigidity), which is equal to $\frac{E_{bo}}{2\ (1 + \nu)}$. The shear deformation of the uncracked concrete is normally neglected.

When the concrete has cracked, the shear strain of course takes on a different value. It is assumed that the shear force is then resisted by compression in a concrete diagonal and tension in the stirrups. This approximation of the pattern of forces in a shear region has long been known as the lattice analogy (see Fig. 37). The theory concerned is presented in Appendix V. The derivation of the formulas is given fairly general in the appendix. Nevertheless the assumption that the compression diagonals of the lattice are inclined at 45^0 is generally a sufficiently accurate one. Furthermore, vertical stirrups are used in the beams considered in this paper. On substitution those two values, the general formulas are greatly simplified. The formula for the shear stiffness in the cracked state becomes then:

$$(GB)_g = \frac{E_a \cdot \omega_t}{4n_o\ \omega_t + k}\ b \cdot z,$$

where

E_a = modulus of elasticity of steel;

ω_t = quantity of stirrup reinforcement expressed as a fraction of the concrete area concerned.

$$\omega_t = \frac{A_t}{b.t} = \frac{\text{cross-sectional area of a stirrup}}{\text{beam-width x stirrup-spacing}};$$

z = lever arm;

$n_o = \frac{E_a}{E'_{bo}}$ = ratio of moduli of elasticity;

$k = 1 - \frac{T_r}{T}$, T_r = the shear force in the part of the beam, when the cracking moment is reached there and

T = the actual shear force.

The ratio k is taken into account because tests have shown that the actual tensile stress in stirrups is lower than may be expected theoretically, as mentioned in Appendix V.

Furthermore, from considerations of equilibrium (also outlined in Appendix V) it appears that, as a result of the shear force, the compressive and the tensile force associated with the bending moment are respectively decreased and increased by an amount equal to $\frac{1}{2}$ T. This amount is also related to vertical stirrups and compression diagonals at an inclination of 45^0.

These changes of the horizontal forces of course also have consequences with regard to the curvature that accurs. The increase in curvature is:

$$\varkappa_t = \frac{T}{2.z}\left\{\frac{1}{A.E_a} - \frac{1}{b.x.E'_{bo}}\right\}$$

where A is the cross-sectional area of the tensile reinforcement and $x\ (= k_x h)$ is the depth of the compressive zone of the concrete. On further working this out we obtain:

$$\varkappa_t = \frac{T}{2k_z\ bh^2}\left\{\frac{1}{\omega E_a} - \frac{1}{k_x.E'_{bo}}\right\}$$

In many cases encountered in actual practice the product $\omega.E_a$ in the above expression has the following value:

$\omega.E_a = 0.007 \times 2.1 \times 10^6 \approx 0.15 \times 10^5$

and:

$k_x.E'_{bo} = 0.3 \times 3 \times 10^5 \approx 1 \times 10^5$ $\quad (\sigma'_w \approx 300\ kg/cm^2)$

The share of the steel in the change of curvature is therefore $\frac{1}{\omega.E_a} \approx 7 \times 10^{-5}$ and that of the concrete is $\frac{1}{k_x.E'_{bo}} \approx 10^{-5}$.

As a result of neglecting the latter, an approximately 15% greater increase in curvature is therefore found. This difference can be compensated by substituting $k_z = 1$ in the denominator of the expression for $\varkappa_t$. Actually this means that the increase in curvature due to shear force is taken as equal to the increase in the steel strain divided by the

effective depth of the beam:

$$\varkappa_t = \frac{T}{2\ \omega\ E_a\ bh^2}$$

Taking account of this shear force effect, the flexural stiffness of the cracked section becomes:

$$(EI)_{gd_i} = \frac{\Delta M}{\Delta\varkappa + \Delta\varkappa_t} = \frac{\frac{\Delta M}{\Delta\varkappa}}{(1 + \frac{\Delta\varkappa_t}{\Delta\varkappa})} = \frac{(EI)_{gd_{i-1}}}{1 + \xi} \qquad \left((EI)_{gd_o} = (EI)_g\right)$$

In these and the following formulas ΔM, ΔT and $\Delta\varkappa$ are the increases of moment, shear force and curvature above the moment where $(EI)_g$ has to be changed. The factor ξ is:

$$\xi = \frac{\Delta\varkappa_t}{\Delta\varkappa} = \frac{\Delta T}{2\omega . E_a . bh^2} \quad \frac{(EI)_g}{\Delta M}$$

or:

$$\xi = \frac{(EI)_g}{2\omega . E_a . bh^2} . \frac{\Delta T}{\Delta M}$$

As an approximation the following expression may be adopted:

$$\xi = \frac{0.48\ E_a . \omega . bh^3}{2E_a . \omega . bh^2} . \frac{\Delta T}{\Delta M} = 0.24\ \frac{\Delta T}{\Delta M}\ h$$

3.2.3. Crack width

The maximum crack width can be calculated with the formulas given in the Netherlands Code of Practice for Reinforced Concrete (GBV). The validity of these formulas in a region of constant bending moment has recently been confirmed by a fairly extensive experimental investigation, the results of which are given in CUR Report No. 37.

The GBV formulas (clause 46-3c) are as follows:

$$w_{max} = \left[0.5\ \sigma_a .\ \ell - 16\ \frac{(\Delta\ell)^2}{\emptyset} \right] 10^{-6}\ \text{cm}$$

where the crack width $\Delta\ell$ is equal to:

$$\Delta\ell = (d_s + 0.3\,\Sigma\emptyset)(1 + 3\sqrt{\frac{1}{n\omega_o}})$$

The steel stress σ_a to be substituted into these expressions is determined from $\sigma_a = M . \frac{\sigma_{ae}}{M_u}$ kg/cm^2.

Approximately the same value for the maximum crack width is obtained with the CEB formula:

$$w_{max} = \left(1.5\ c + 0.16\ \frac{b_o \cdot h}{n \pi \phi} \right) \left(\sigma_a - 16\ \frac{b_o \cdot h}{n \pi \phi^2} \right) \cdot 10^{-6}\ \text{cm}$$

In those regions where the shear force plays a significant part the maximum crack width can no longer be calculated by means of the GBV formula. The widths that actually occur can be much greater than indicated by this calculation. Accordingly, in such regions the crack width is calculated from the curvature that occurs there. The basic assumption made for this purpose is that the curvature which develops over the crack spacing manifests itself entirely as a rotation by the distance between the tensile fibre and the neutral axis. A value of 0.7 h is adopted for this distance. Hence:

$$w_{max} = \varkappa \cdot \Delta\ell \cdot 0.7\ h \quad \text{cm}$$

The crack spacing $\Delta\ell$ in such cases can, however, be calculated with the mentioned formula given in GBV - code of practice.

4. Comparison of measured and calculated values

The results of the experimental investigation concerning the two-span reinforced concrete beams, discussed in chapter 2, will now be compared with the results of calculations according to chapter 3 of this paper. The comparison is presented in Figs. 38 to 40 for beam B1 to B3 respectively. Those diagrams show the bending moment distribution, the deflection and the maximum crack width as functions of the loading acting upon the beam.

As mentioned before the first calculations were carried out without taking into account the effect of shear force. As can be seen in the diagrams mentioned above, the comparison of the measured and calculated values revealed considerable discrepansies. The differences concern the moment distribution, the deflections and the crack widths at the interior support. The more the distribution of the reinforcement deviates from the distribution of the elastic-moments the greater are the differences.

The relative great difference between the measured values and the first calculations with respect to the deflections is striking. Altogether this led to the conclusion that the shear effects had wrongly been neglected.

The results after taking into account the shear force effects according to chapter 3.2 were remarkably better. There is now reasonable good agreement between the measured and the calculated moments and deflections. This is clearly apparent from the diagrams concerned in Figs. 38 to 40. (The deflection diagrams also include the calculated results for the deflection neglecting the extra caused by the shear deformation of the beam, but including the correction of the flexural stiffness with regard to shear.)

With regard to the maximum crack width at the interior support it is clearly apparent also that the CEB- and GBV formula as well, are quite unsuitable for that region of the beam. With the calculation of the crack width from the curvature that occurs there, values are obtained which approximate reality much better. A phenomenon not solved by the revised calculation is the fact that in the tests of beam B2 and B3 the yield moment at the interior support and after that the span moment, reaches a higher value than the theoretical one. On the contrary the agreement between both values was very good for beam B1 and B4 and also for test beams A1 and A2 used to measure the M-$\varkappa$ diagrams of the sections concerned.

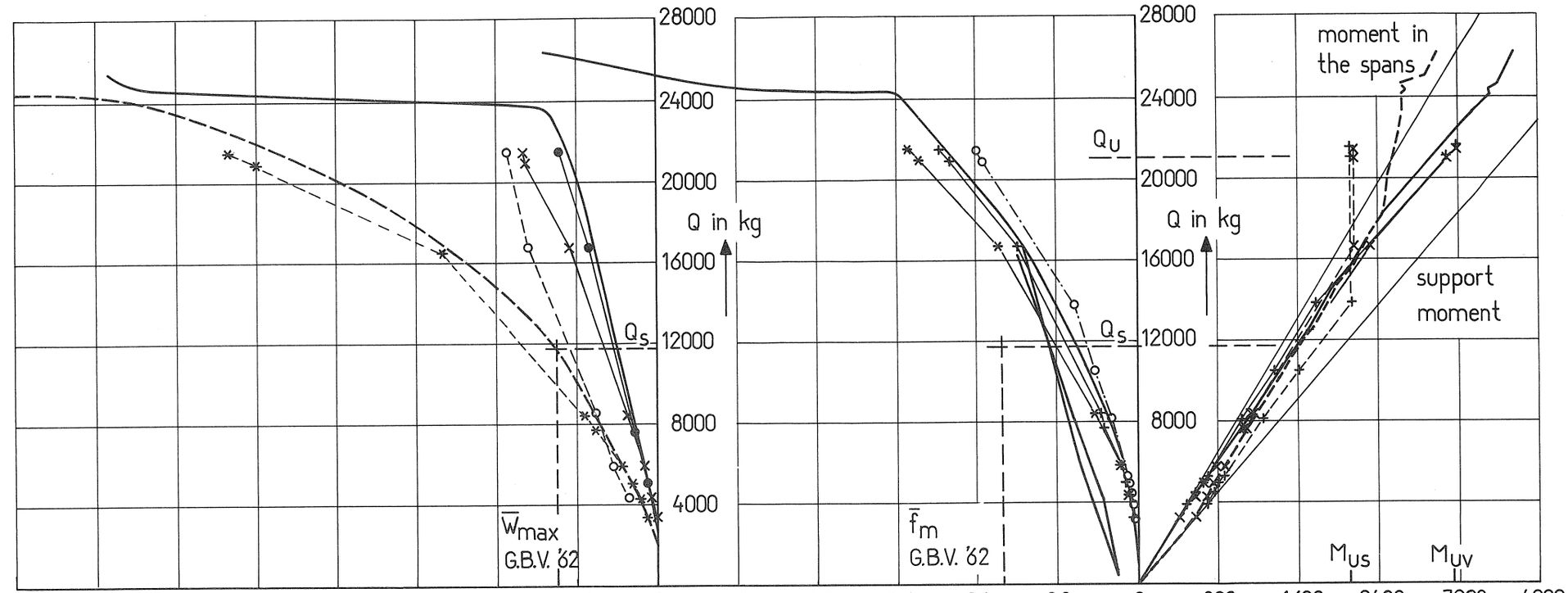

Fig. 39. Beam B_2.
Comparison calculated and measured values.

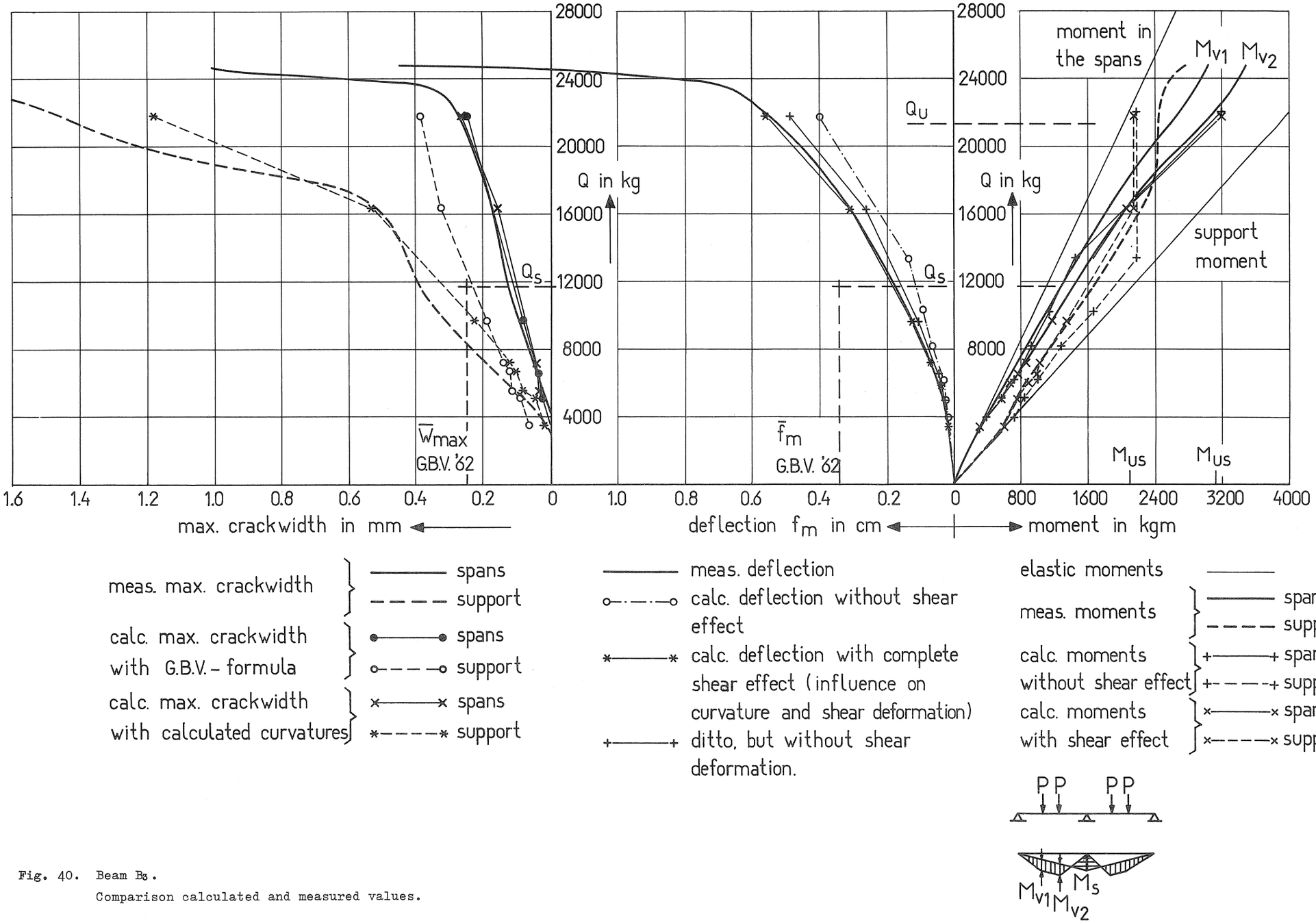

Fig. 40. Beam B_3.
Comparison calculated and measured values.

Although the differences are relatively very small, this phenomenon of apparently low steel stresses therefore is striking, because this result is opposite to what could be expected with regard to the shear in that region. The effect of bond-slip could be an explanation for those differences. Otherwise bond-slip has the same effect as what is called shear force effect in this paper. If one would take this into account, however, a complete new calculation procedure must be developed.

As a further comparison of measured and calculated values the curvatures that occur along the length of the B beams concerned were plotted into diagrams. The results of this are presented for beam B3 in Figs. 42 to 47 (Fig. 41 gives an explanation of the symbols used). In the figures the average curvatures in each beam element (the latter obtained from the sub-division of the beam into elements with regard to the calculation) is plotted against the average moment in that part of the beam. Both measured and calculated values are given; for completeness the actual shear force is noted down too. The diagrams concerning the other beams B1 and B2 are showing about the same agreement; they are not presented in this paper.

Having regard to the fact that the calculation must always be to some extend constitute an idealisation of reality, the agreement between the calculated and the measured curvatures and shear forces can be described as good. Figs. 43 and 44 give rise to the remark that a 'falling branch' occurs in the region of the beam near the interior support. This is simply a consequence of the fact, that while the support moment has a constant value after reaching the yield moment, the moment in the span is still increasing. The zero point of bending moment moves in the direction of the central support. Therefore the average moment in the beam element besides that support is decreasing.

In conclusion, from the above, it can be inferred that the principles and basic features introduced into the calculations do indeed provide a reasonable good representation of the really significant factors. However, one could well imagine that in a case of very good bond properties the influence of shear is less than shown in this paper. The given calculation procedure provides for these cases values which lay on the safe side, especially with regard to the crack widths near the interior support. The latter being decisive for the service-ability in most practical cases where the distribution of the reinforcement is not

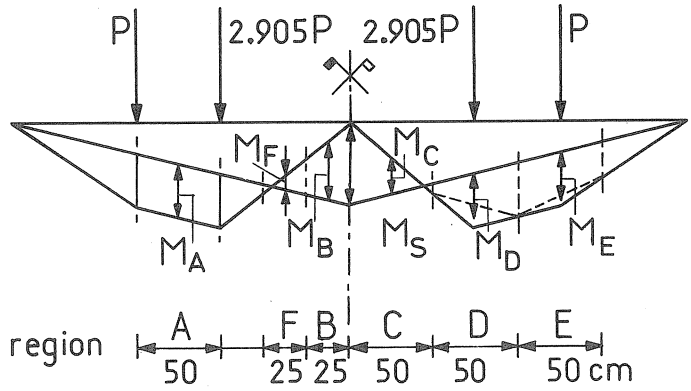

Fig. 41. Beam-regions.

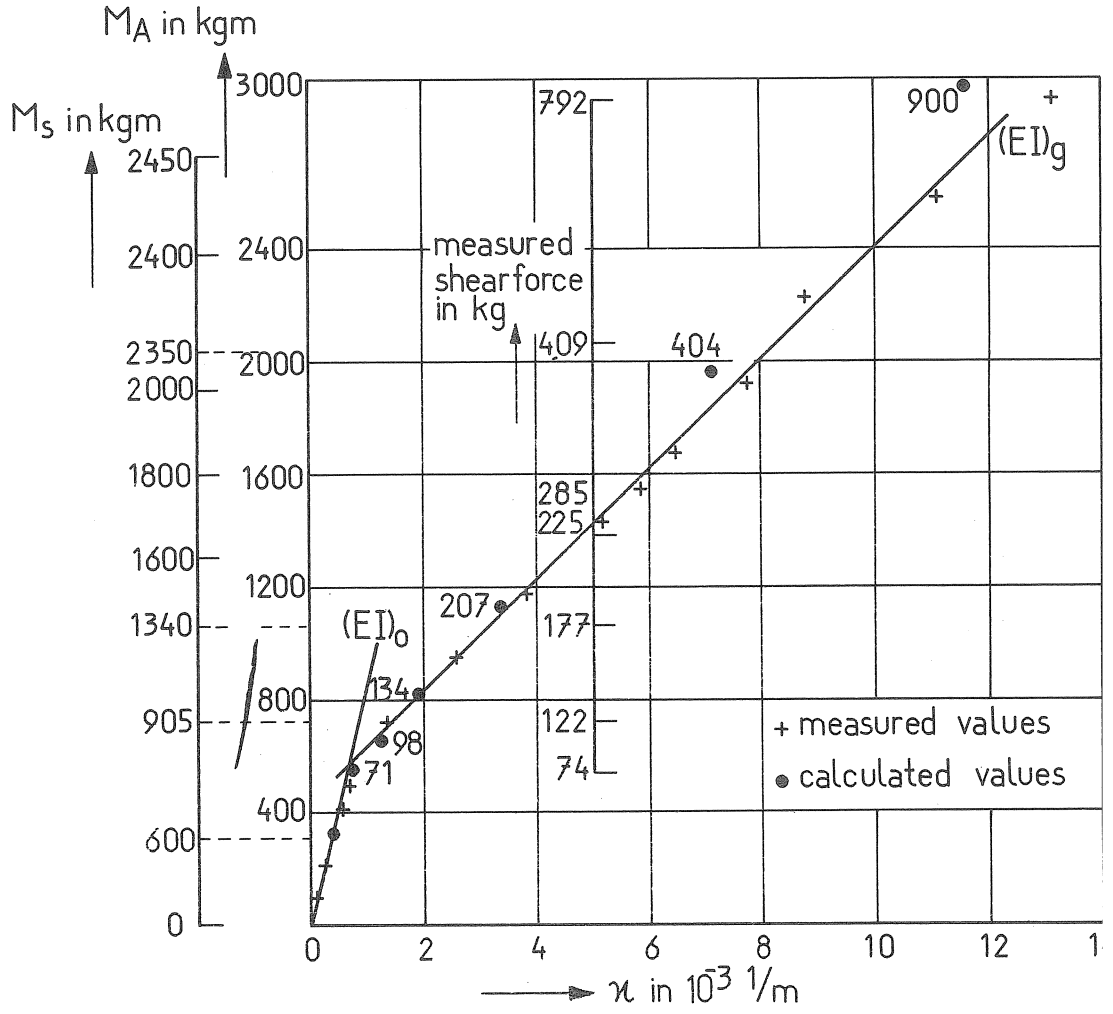

Fig. 42. Beam B_3.
Comparison of average curvature and shear force in region A.

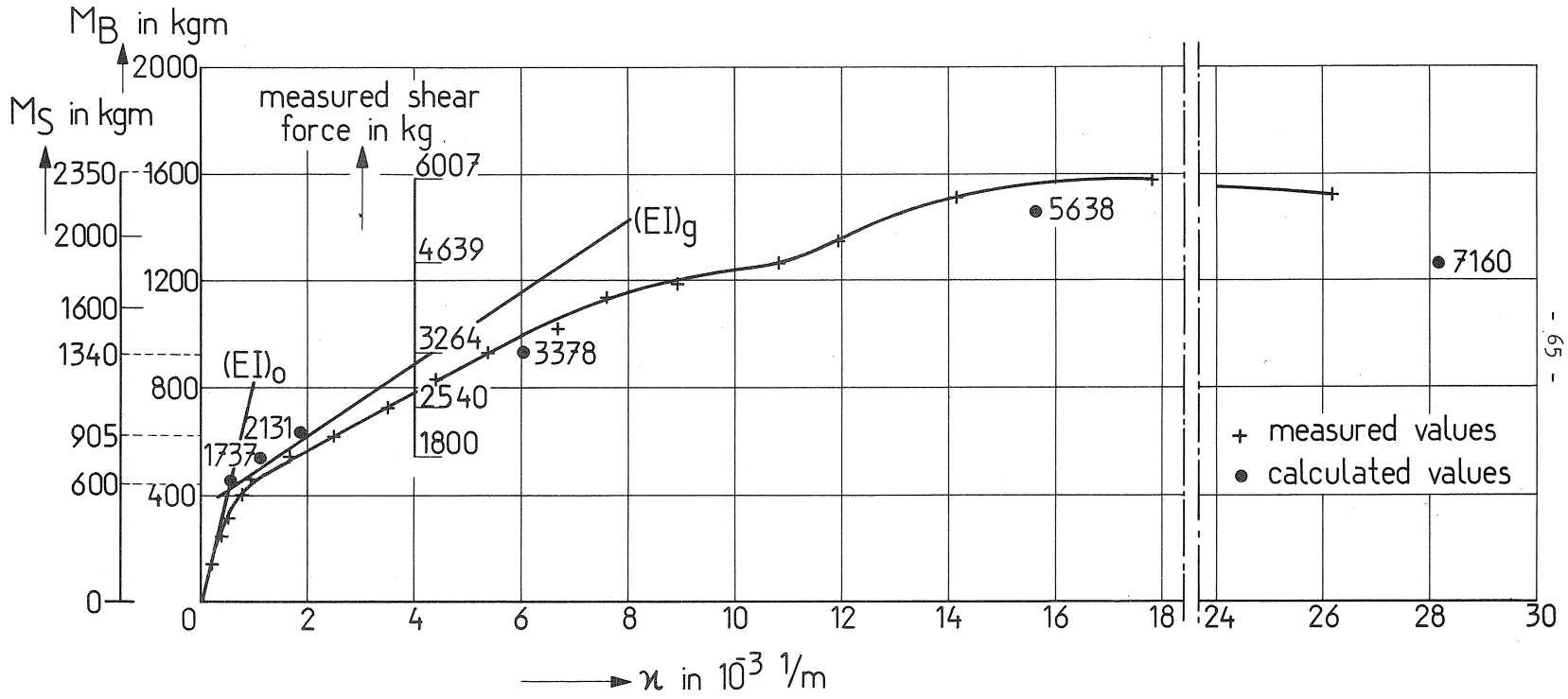

Fig. 43. Beam B_3. Comparison of average curvature and shear force in region B.

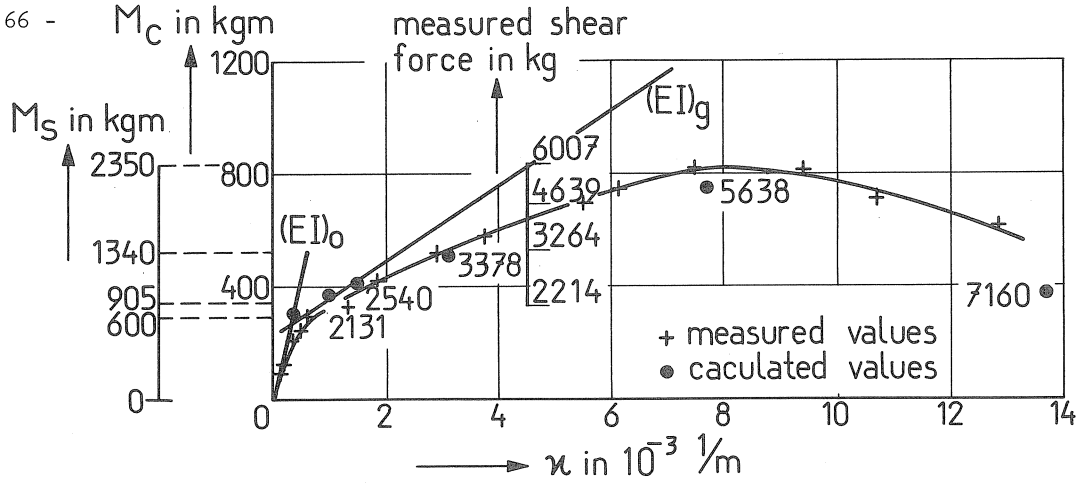

Fig. 44. Beam B3, region C.

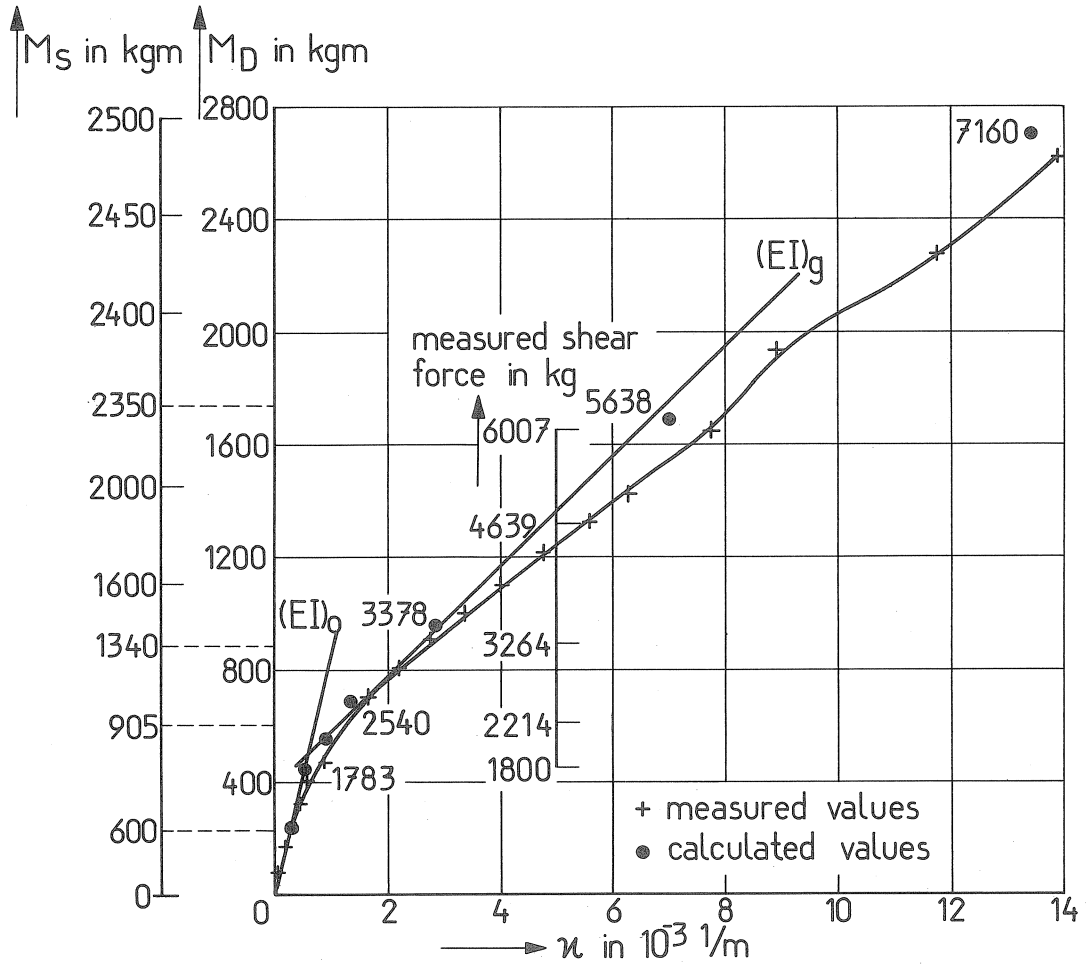

Fig. 45. Beam B3.
Comparison of average curvature and shear force in region D.

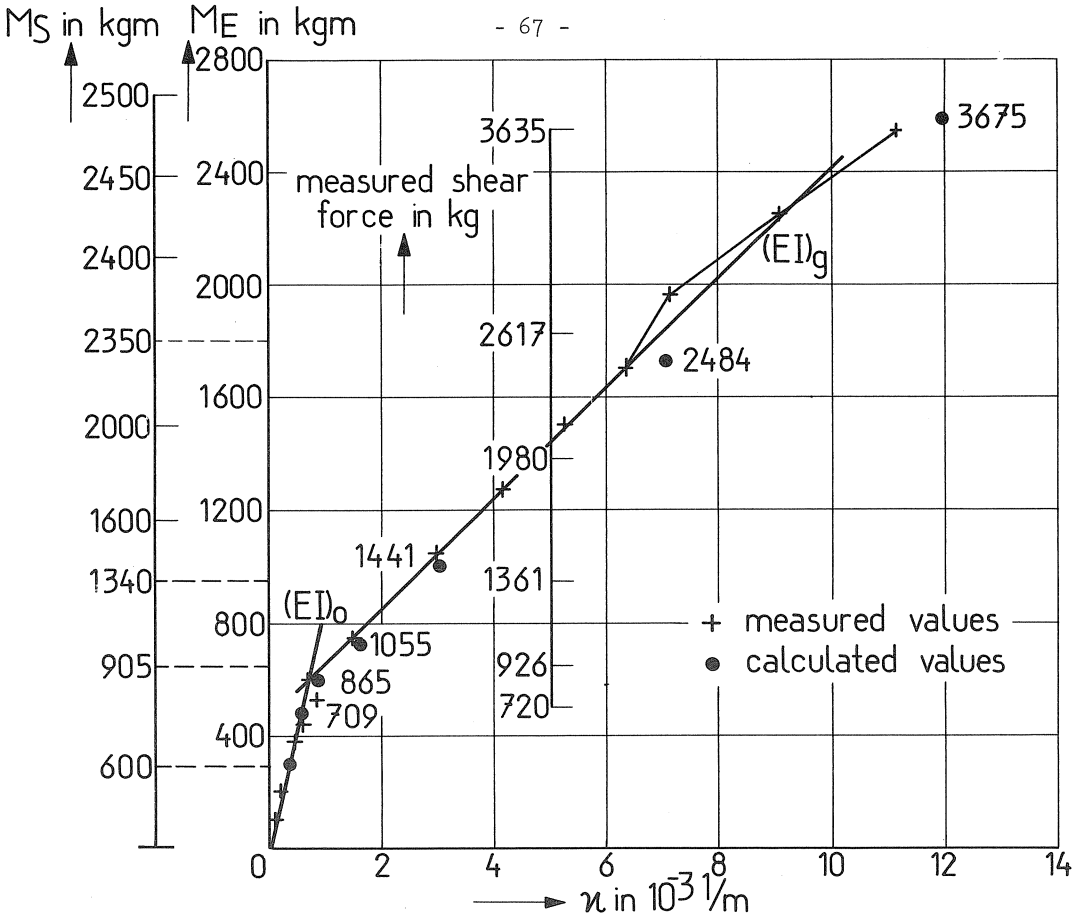

Fig. 46. Beam B3, region E.

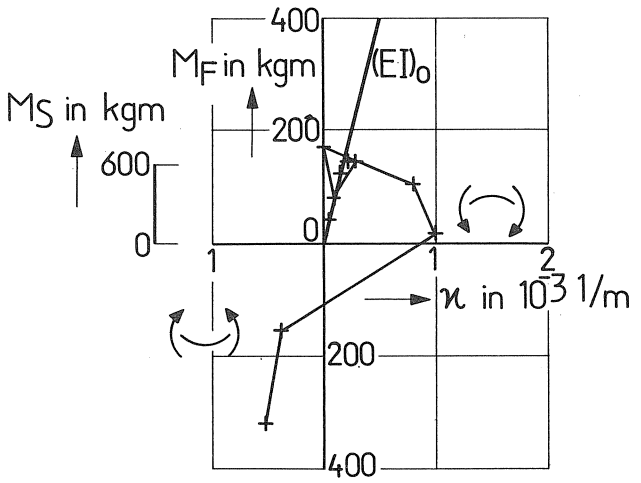

Fig. 47. Beam B3.
Comparison of average curvature and shear force in region F.

in agreement with the distribution of the elastic moments (in this way that support reinforcement is transferred).

Therefore it was decided to carry out the further calculations of our investigation in correspondence with the procedure discussed in this paper. These calculations must, as mentioned in the introduction, lead to real numbers for the limitting factors concerning the distribution of reinforcement in 'hyperstatique' structures with regard to the service ability requirements. At the moment these calculations are being carried out.

Acknowledgments

This study has been carried out in the laboratories of the Institute for Building Materials and Building Structures TNO-IBBC in Delft, and was supported by the Netherlands Committee for Concrete Research CUR. Especially CUR-working groupe A 19 was involved in the investigation. Several research workers of the Institute collaborated in the research, Ir. J. Blaauwendraad programmed the analysis procedure for the computer. P.W. van de Haar assisted with the experimental investigation and in preparing this paper as well.

This paper summarises several TNO-reports, namely:

1. concerning the M-$\varkappa$ diagram of reinforced concrete:
   reports no. BI-65-1, 10 parts (November 1965), BI-66-49 (July 1966), BI-67-106 (October 1967), BI-67-110 (December 1967);
2. concerning the computer-analysis:
   report no. BI-66-67 (October 1966);
3. concerning the tests on the continuous beams:
   reports no. BI-67-109 (December 1967), BI-69-7 (January 1969).

Appendix I. Calculation of the elastic distribution of moments.

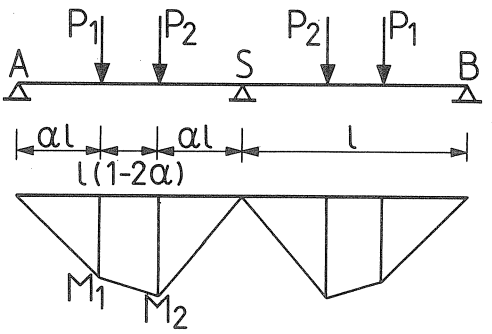

area of moment diagram of statically determined primary system

$$M_1 = \left\{ P_1 + \alpha(P_2 - P_1) \right\} \alpha\ell$$

$$M_2 = \left\{ P_2 + \alpha(P_2 - P_1) \right\} \alpha\ell$$

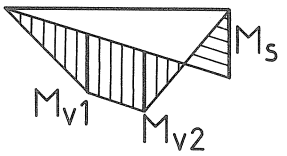

The angular rotation due to applied loads: $\frac{1}{2} EI \varphi_s = \frac{1}{6}\alpha\ell^2 (1-\alpha)\left\{P_1 (1+\alpha) + P_2(2-\alpha)\right\}$

due to M_s : $\frac{1}{2} EI \varphi_s = \frac{1}{3} M_s \ell$

from which:

$$M_s = \frac{1}{2} \alpha\ell(1-\alpha) \left\{P_1 (1+\alpha) + P_2 (2 - \alpha)\right\} \tag{1}$$

Then the moments in the spans:

$$M_{v1} = \frac{1}{2} \alpha\ell \left\{P_1 (2-3\alpha+\alpha^3) + P_2 (3\alpha^2 - \alpha^3)\right\} \tag{2}$$

$$M_{v2} = \frac{1}{2} \alpha\ell \left\{P_1 (-1+3\alpha+\alpha^2 - \alpha^3) + P_2 (3\alpha - 4\alpha^2 + \alpha^3)\right\} \tag{3}$$

From the equation (1) and (2) the ratio of max. moments is:

$$\frac{M_{v1}}{M_s} = \frac{P_1 (2-3\alpha+\alpha^3) + P_2 (3\alpha^2 - \alpha^3)}{P_1 (1+\alpha) + P_2 (2-\alpha)} \tag{4}$$

Suppose that between the two point loads the resultant moment must be constant, then follows from the equations (2) and (3) the condition:

$$P_2 = \frac{3-\alpha^2}{\alpha(3-\alpha)} P_1 \tag{5}$$

Beams B_1, B_2 and B_4:

$$\ell = 2 \text{ m}$$
$$\alpha = \frac{3}{8}$$
$$P_1 = P_2 = \frac{1}{4} Q$$

$$M_s = 0.704 P = 0.176 Q \qquad \text{eq. (1)}$$
$$M_{v_1} = 0.486 P = 0.122 Q \qquad \text{eq. (2)}$$
$$M_{v_2} = 0.310 P = 0.078 Q \qquad \text{eq. (3)}$$
$$\frac{M_{v_1}}{M_s} = 0.690 \qquad \text{eq. (4)}$$

Beam B_3:

$$\ell = 2 \text{ m}$$
$$\alpha = \frac{3}{8}$$
$$P_2 = 2.905 P_1 \begin{cases} P_1 = 0.128 Q \\ P_2 = 0.372 Q \end{cases} \qquad \text{eq. (5)}$$

$$M_s = 1.429 P_1 = 0.183 Q \qquad \text{eq. (1)}$$
$$M_{v_1} = M_{v_2} = 0.750 P_1 = 0.096 Q \qquad \text{eq. (2) and (3)}$$
$$\frac{M_{v_1}}{M_s} = \frac{M_{v_2}}{M_s} = 0.525 \qquad \text{eq. (4)}$$

Appendix II. Calculation of the yield moment.

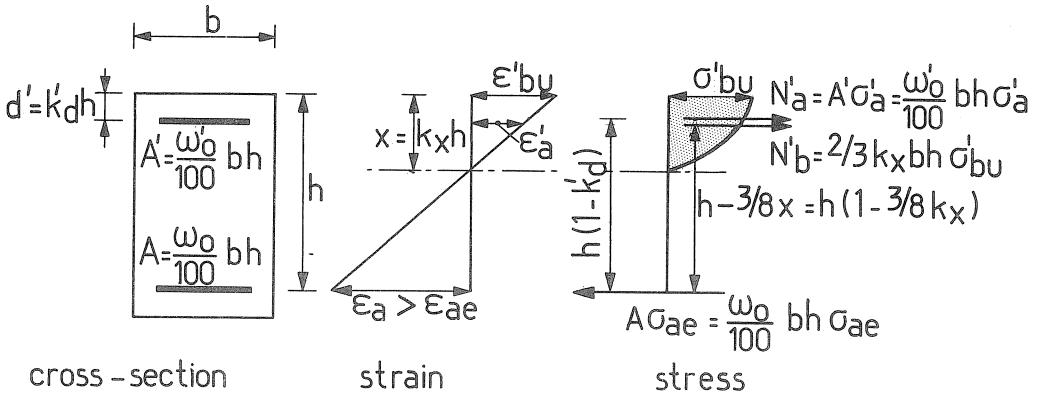

From the strain distribution:

$$\varepsilon'_a = \varepsilon'_{bu} \frac{x-d'}{x} = \varepsilon'_{bu} \left(1 - \frac{k'_d}{k_x}\right) \tag{1}$$

and thus

$$\sigma'_a = \varepsilon'_{bu} E_a \left(1 - \frac{k'_d}{k_x}\right) \leqq \sigma'_{ae} \tag{2}$$

From equality of total tensile and compressive forces follows:

$$N'_b + N'_a - N_a = 0 \tag{3}$$

$$\frac{2}{3} k_x \sigma'_{bu} + \frac{\omega'_o}{100} \varepsilon'_{bu} E_a \left(1 - \frac{k'_d}{k_x}\right) - \frac{\omega_o}{100} \sigma_{ae} = 0 \tag{4}$$

$$k_x^2 + k_x \frac{3\omega_o}{200\sigma'_{bu}} \left(\frac{\omega'_o}{\omega_o} \varepsilon'_{bu} E_a - \sigma_{ae}\right) - \frac{3\omega_o}{200\sigma'_{bu}} \left(\frac{\omega'_o}{\omega_o} \varepsilon'_{bu} E_a k'_d\right) = 0 \tag{5}$$

from which:

$$k_x = -\frac{3\omega_o}{400\sigma'_{bu}} \left(\frac{\omega'_o}{\omega_o} \varepsilon'_{bu} E_a - \sigma_{ae}\right) \left[1 - \sqrt{1 + \frac{2 \frac{\omega'_o}{\omega_o} \varepsilon'_{bu} E_a k'_d}{\frac{3\omega_o}{400\sigma'_{bu}} \left(\frac{\omega'_o}{\omega_o} \varepsilon'_{bu} E_a - \sigma_{ae}\right)^2}}\right] \tag{6}$$

The bending moment is

$$M_u = \left[\frac{2}{3} k_x \left(1 - \frac{3}{8} k_x\right) \sigma'_{bu} + \frac{\omega'_o}{100} \left(1 - \frac{k'_d}{k_x}\right)\left(1 - k'_d\right) \varepsilon'_{bu} E_a\right] bh^2 \tag{7}$$

If $\varepsilon'_{bu} E_a \left(1 - \frac{k'_d}{k_x}\right) \geqq \sigma'_{ae}$ (8)

then follows, with equation (3) and $\sigma'_a = \sigma'_{ae} = \sigma_{ae}$, (9)

from equilibrium conditions:

$$\frac{2}{3} k_x \sigma'_{bu} - \frac{\sigma_{ae}}{100} (\omega_o - \omega'_o) = 0$$

$$k_x = \frac{3(\omega_o - \omega'_o)}{200} \frac{\sigma_{ae}}{\sigma'_{bu}} \tag{10}$$

Equation (7) becomes in this case

$$M_u = \left[\frac{2}{3} k_x \left(1 - \frac{3}{8} k_x\right) \sigma'_{bu} + \frac{\omega'_o}{100} \left(1 - k'_d\right) \sigma_{ae}\right] bh^2 \qquad (11)$$

Substitution of:

$\varepsilon'_{bu} = 3.5‰$

$\sigma'_{bu} = 0.6 \times 315 = 189$ kg/cm^2 (table 1: 20 cm cubes)

$E_a = 2.03 \times 10^6$ kg/cm^2 } (Fig. 6)

$\sigma_{ae} = \sigma'_{ae} = 4350$ kg/cm^2 }

in the equations (6), (8) and (7) yields for

$\frac{\omega'_o}{\omega_o} = \frac{3}{2}$: $k_x = 0.125$ (x = 2.95 cm)

$\sigma'_a = 1334$ kg/cm^2

$M_u = 2155$ kgm

$\frac{\omega'_o}{\omega_o} = \frac{2}{3}$: $k_x = 0.181$ (x = 4.28 cm)

$\sigma'_a = 3118$ kg/cm^2

$M_u = 3187$ kgm

Appendix III. Calculation of the moments from the support reactions.

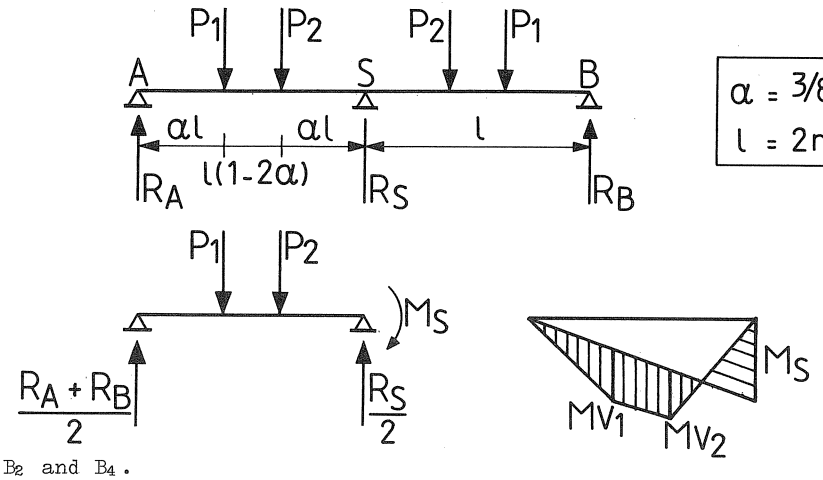

Beams B_1, B_2 and B_4.

$$R_A + R_B = 2\left\{P_1(1-\alpha) + P_2\alpha - \frac{M_s}{\ell}\right\} = \frac{1}{4}\left\{5P_1 + 3P_2 - 4M_s\right\} \quad (1)$$

$$Q = 2(P_1 + P_2) = R_A + R_B + R_S \quad (2)$$

Combining Eq. (1) and (2), and substitution $P_1 = P_2$:

$$M_s = \frac{1}{2}\left\{R_S - (R_A + R_B)\right\} \quad (3)$$

The moments in the spans become

$$M_{v1} = \frac{1}{2}\alpha\ell\,(R_A + R_B) = \frac{3}{8}(R_A + R_B) \quad (4)$$

$$M_{v2} = \frac{1}{2}R_S\,\alpha\ell - M_s = \frac{1}{4}\ell\left\{(R_A + R_B) - R_S(1 - 2\alpha)\right\} \quad (5)$$

$$= \frac{1}{2}(R_A + R_B) - \frac{1}{8}R_S.$$

Beam B_3.

Substitution:

$$P_2 = 2.905\,P_1 \quad (6)$$

and

$$Q = 2(P_1 + P_2) = 7.81\,P_1 = R_A + R_B + R_S \quad (7)$$

in Eq. (1) yields:

$$M_s = 0.439\,R_S - 0.561\,(R_A + R_B) \quad (8)$$

Finally is:

$$M_{v1} = M_{v2} = 0.375\,(R_A + R_B) \quad (9)$$

Appendix IV. Calculation of the failure load.

Beam B_1, B_2 and B_4.

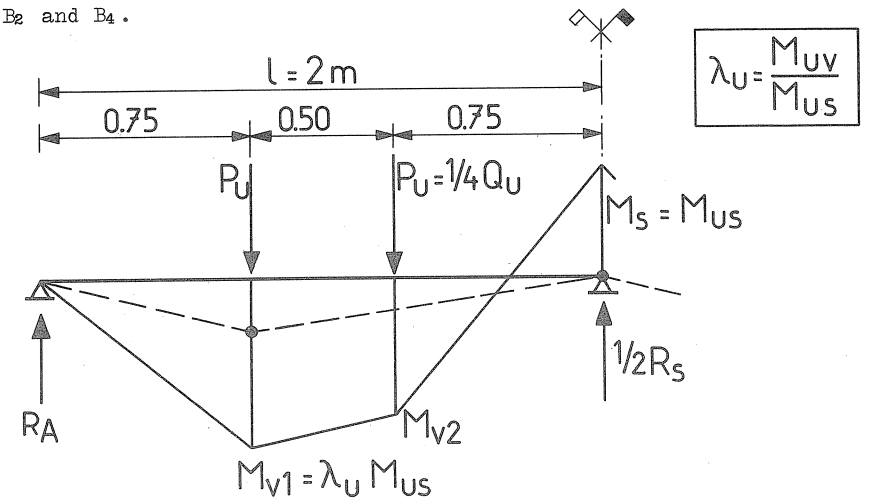

$$R_A = P_u - \frac{1}{2} M_{us} \qquad (1)$$

$$M_{v_1} = M_{uv} = \lambda_u M_{us} \qquad (M_u = \text{yield moment, see appendix II}) \qquad (2)$$

$$M_{v_1} = 0.75\, R_A = \frac{3}{4} \left(P_u - \frac{1}{2} M_{us}\right) \qquad (3)$$

From equations (2) and (3) follows

$$P_u = \frac{1}{6} M_{us} \left(8\lambda_u + 3\right) \qquad (4)$$

or

$$Q_u = \underline{\underline{\frac{2}{3} M_{us} \left(8\lambda_u + 3\right)}} \qquad (5)$$

That yields

$$R_A = \frac{4}{3} \lambda_u M_{us} \qquad (6)$$

and

$$M_{v_2} = \frac{4}{3} \lambda_u M_{us} \frac{5}{4} - \frac{1}{6} M_{us} \left(8\lambda_u + 3\right)\frac{1}{2} = \frac{1}{4} M_{us} \left(4\lambda_u - 1\right) \qquad (7)$$

Beam B_3.

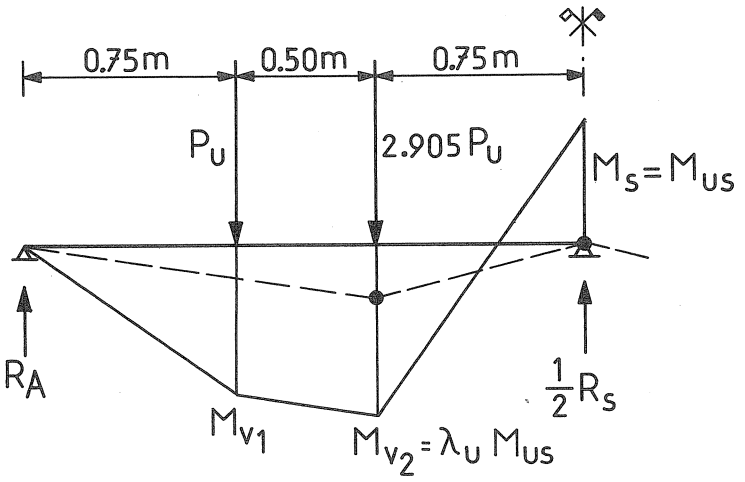

$$R_A = \frac{1}{2}\,(1.25\,P_u + 0.75 \times 2.905\,P_u - M_{us}) =$$

$$= \frac{1}{2}(3.4288\,P_u - M_{us}) \qquad (8)$$

$$M_{v2} = M_{uv} = \lambda_u\,M_{us} \qquad (9)$$

$$M_{v2} = 1.25\,R_A - 0.50\,P_u = \frac{5}{8}(2.629\,P_u - M_{us}) \qquad (10)$$

From equations (9) and (10) follows

$$P_u = \frac{8\lambda_u + 5}{13.144}\,M_{us} = 0.076\,M_{us}\,(8\lambda_u + 5) \qquad (11)$$

or

$$Q_u = 7.81\,P_u = \underline{\underline{0.594\,M_{us}\,(8\lambda_u + 5)}} \qquad (12)$$

That yields

$$R_A = 0.1304\,M_{us}\,(8\lambda_u + 5) - 0.5\,M_{us} = 0.1304\,(8\lambda_u + 1.167)M_{us} \qquad (13)$$

and

$$M_{v1} = 0.75\,R_A = 0.0978\,M_{us}\,(8\lambda_u + 1.167) \qquad (14)$$

Appendix V

CALCULATIONS CONCERNING THE EFFECT OF SHEAR ON THE BEHAVIOUR OF A CRACKED REINFORCED CONCRETE BEAM

The theory concerned was earlier discussed by Mörsch, Kupfer and Dilger *).

The deformations due to shear force in cracked concrete are investigated with reference to the beam portion represented in fig. V-1. The deformations which occur can be plotted in a Williot diagram with the intersection of stirrup and compression diagonal as the fixed point (see fig. V-1^b); then:

$$\psi \approx \operatorname{tg} \psi = \frac{\varepsilon_a}{\sin^2\alpha(\operatorname{ctg}\alpha + \operatorname{ctg}\beta)} + \frac{\varepsilon'_b}{\sin^2\beta(\operatorname{ctg}\alpha + \operatorname{ctg}\beta)}$$

where ψ is the shear strain, ε_a is the tensile strain in the stirrup, ε'_b is the compressive strain in the compression diagonal, β is the angle of the compression diagonal and α is the angle of the stirrup with respect to the axis of the beam.

From the vertical equilibrium conditions (see fig. V-1^c) it is now obtained for the "diagonal tension":

$$T_a = \frac{T}{\sin\alpha}$$

while the total cross-sectional area of the stirrups in the section concerned is:

$$A_a = \frac{A_t \cdot z(\operatorname{ctg}\alpha + \operatorname{ctg}\beta)\sin\alpha}{t \sin\alpha}$$

where A_t is the cross-sectional area of a stirrup (two-leg or four-leg) and t is the (horizontal) stirrup spacing.

If the quantity of stirrup reinforcement is expressed as a fraction of the concrete area, namely:

$$\omega_t = \frac{A_t}{b.t.\sin\alpha}$$

*) Kupfer, H.:
Erweiterung der Mörsch' sehen Fachwerkanalogie mit Hilfe des Prinzips vom Minimum der Formänderungsarbeit;
CEB - Bulletin d'Information, nr. 40, Jan. 1964.

Dilger, W.:
Veränderlichkeit der Biege- und Schubsteifigkeit bei Stahlbetontragwerken und ihr Einfluss auf Schnittkraftverteilung und Traglast bei statisch unbestimmter Lagerung;
Deutscher Ausschuss für Stahlbeton. Heft 179, 1966.

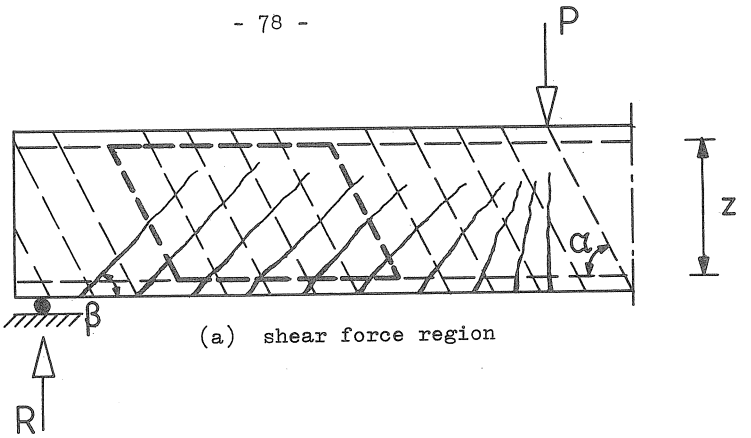

(a) shear force region

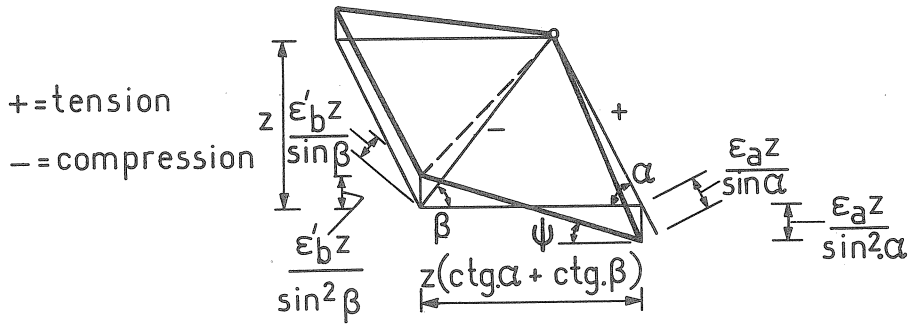

(b) deformations

section along the compression diagonal (at an angle β)

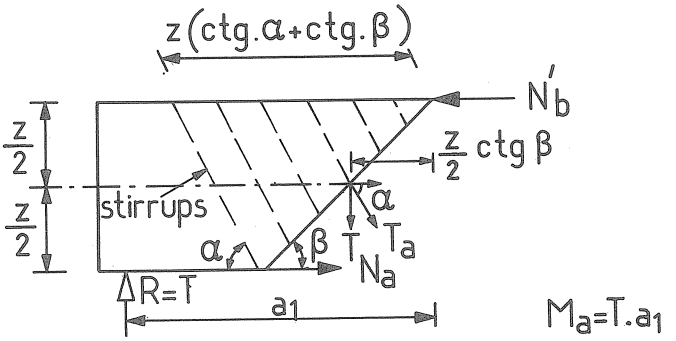

section along a stirrup (at an angle α)

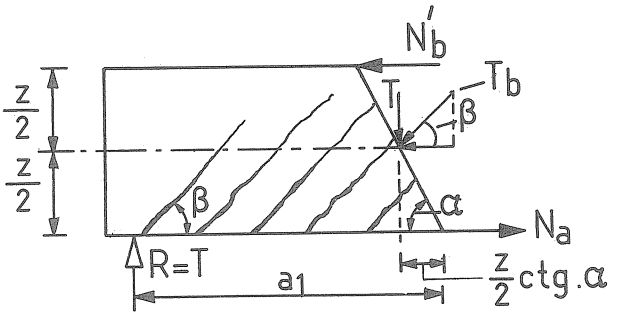

(c) forces acting

Fig. V-1.

then:

$$A_a = \omega_t . b.z(\mathrm{ctg}\,\alpha + \mathrm{ctg}\,\beta)\sin\alpha .$$

Now the (tensile) strain of the stirrup can be calculated:

$$\varepsilon_a = \frac{T_a}{E_a . A_a} = \frac{T}{E_a . \omega_t . b.z(\mathrm{ctg}\,\alpha + \mathrm{ctg}\,\beta)\sin^2\alpha}$$

The (compressive) strain of the compression diagonal can be calculated in approximately similar fashion.

Consider the vertical equilibrium (fig. V-1^c, lower diagram):

$$T_b = \frac{T}{\sin\beta} .$$

The cross-sectional area of a compression diagonal is:

$$B = b.z(\mathrm{ctg}\,\alpha + \mathrm{ctg}\,\beta)\sin\beta .$$

We thus obtain:

$$\varepsilon'_b = \frac{T_b}{E'_{bo} . B} = \frac{T}{E'_{bo} . b.z(\mathrm{ctg}\,\alpha + \mathrm{ctg}\,\beta)\sin^2\beta}$$

On substitution of these values of ε_a and ε'_b into the expression for the shear strain, it follows:

$$\psi = \frac{T}{b.z(\mathrm{ctg}\,\alpha + \mathrm{ctg}\,\beta)^2} \left\{ \frac{1}{E_a . \omega_t . \sin^4\alpha} + \frac{1}{E'_{bo}\,\sin^4\beta} \right\}$$

For the uncracked concrete the shear strain was:

$$\psi = \frac{T}{(G.B)_o}$$

so that, corresponding to this expression, the shear stiffness for the cracked concrete is:

$$(G.B)_g = \frac{E_a . \omega_t . E'_{bo} . \sin^4\beta\,(\mathrm{ctg}\,\alpha + \mathrm{ctg}\,\beta)^2}{E_a . \omega_t . \sin^4\alpha + E'_{bo}\,\sin^4\beta} . b.z.$$

Putting $n_o = E_a / E'_{bo}$, this becomes:

$$(G.B)_g = \frac{E_a . \omega_t . \sin^4\alpha . \sin^4\beta (\mathrm{ctg}\,\alpha + \mathrm{ctg}\,\beta)^2}{n_o . \omega_t . \sin^4\alpha + \sin^4\beta} \quad b.z.$$

The assumption that the compression diagonals of the lattice are inclined at 45° (i.e., $\beta = 45^\circ$) is generally a sufficiently accurate one. Furthermore, vertical stirrups are normally employed.

On substitution of $\alpha = 90^\circ$ and $\beta = 45^\circ$ the formula for $(G.B)_g$ is greatly simplified, namely:

$$(G.B)_g = \frac{E_a . \omega_t}{4\, n_o . \omega_t + 1} . b.z.$$

From tests*) it has been established that the steel stress in the stirrups is:

$$\sigma_{at} = \frac{\tau_0 - \tau_{0,s}}{\omega_t}$$

where τ_0 = the shear stress determined by the expression $\frac{T}{b.z}$ and $\tau_{0,s}$ = the shear stress associated with the development of the inclined cracks. This signifies in fact that the stress in the stirrups prior to cracking may be neglected.

From the literature already referred to, it appears that $\tau_{0,s} = \frac{1}{30}\sigma'_w$ provides the best agreement between the measured results and the calculated results.

Having regard to the above, the steel strain occuring in the formula for $(G.B)_g$ should be reduced by a factor:

$$k = \frac{\tau_0 - \tau_{0,s}}{\tau_0}$$

In our computation programme this has been approximated as:

$$k = 1 - \frac{T_r}{T}$$

where T_r is the shear force in the part of the beam concerned, when the cracking moment is reached there.

The formula for the shear stiffness in the cracked state becomes:

$$(G.B)_g = \frac{E_a.\omega_t}{4\, n_o.\omega_t + k} \cdot b.z.$$

The effect of the shear force upon the horizontal compression resultant and the horizontal tension resultant (the forces associated with bending of the beam) follows from further considerations of equilibrium with reference to fig. V-1^c.

*) Leonhardt, F. and Walther, R.:

1) Schubversuche an einfeldrigen Stahlbetonbalken mit und ohne Schubbewehrung;
Deutscher Ausschuss für Stahlbeton, Heft 151
2) Versuche an Plattenbalken mit hoher Schubbeanspruchung;
Deutscher Ausschuss für Stahlbeton, Heft 152
3) Schubversuche an Plattenbalken mit unterschiedlicher Schubbewehrung;
Deutscher Ausschuss für Stahlbeton, Heft 156

Leonhardt, F., Walther, R. and Dilger, W.:
Schubversuche an Durchlaufträgern;
Deutscher Ausschuss für Stahlbeton, Heft 163

From the horizontal equilibrium in the upper diagram of fig. V-1^c we obtain:

$$N_a = N'_b - T_a \cos \alpha$$

and from the equilibrium of moments (with respect to the point of application of N'_b):

$$M_a - N_a \cdot z - T_a \cos \alpha \cdot 1/2\ z - T \cdot 1/2\ z \cdot \operatorname{ctg} \beta = 0$$

Earlier on we had already obtained:

$$T_a = \frac{T}{\sin \alpha}$$

From these three equations it follows that:

$$M_a - N'_b \cdot z + T \cdot z \operatorname{ctg} \alpha - 1/2\ T \cdot z \operatorname{ctg} \alpha - 1/2\ T \cdot z \operatorname{ctg} \beta = 0$$

or: $$N'_b = \frac{M_a}{z} - \frac{T}{2}(\operatorname{ctg} \beta - \operatorname{ctg} \alpha)$$

On similarly considering the equilibrium conditions with reference to the lower diagram of fig. V-1^c, we obtain:

$$N'_b = N_a - T_b \cos \beta$$

where, as already earlier obtained:

$$T_b = \frac{T}{\sin \beta}$$

Furthermore, the equilibrium of moments about the point of application of N_a is:

$$M_a - N'_b \cdot z - T_b \cos \beta \cdot 1/2\ z - T \cdot 1/2\ z \operatorname{ctg} \alpha = 0$$

From these three equations it follows that:

$$M_a - N_a \cdot z + T \cdot z \operatorname{ctg} \beta - 1/2\ z \cdot T \operatorname{ctg} \beta - 1/2\ T \cdot z \operatorname{ctg} \alpha = 0$$

or: $$N_a = \frac{M_a}{z} + \frac{T}{2}(\operatorname{ctg} \beta - \operatorname{ctg} \alpha)$$

From the above considerations of equilibrium it thus appears that, as a result of the shear force, the compressive and the tensile force associated with the bending moment are respectively decreased and increased by an amount equal to

$$\Delta N = \frac{T}{2}(\operatorname{ctg} \beta - \operatorname{ctg} \alpha)$$

With the assumed $\beta = 45^o$ and $\alpha = 90^o$ it follows

$$\Delta N = 1/2\ T.$$

Samenvatting

In deze publikatie wordt een overzicht gegeven van experimenteel en theoretisch onderzoek van doorgaande balken in gewapend beton. Begonnen wordt met een algemene beschouwing over het gedrag van dit type konstrukties. Vervolgens worden de uitgevoerde proeven besproken. Deze betreffen liggers op 3 steunpunten. De berekeningsmethode wordt daarna uiteengezet. In deze methode kan de invloed van de dwarskracht worden meegenomen. De gemeten en berekende waarden worden tenslotte vergeleken.

Het onderzoek leidt tot de konklusie dat de dwarskracht-invloed in de berekening van de vervormingen en de momentenverdeling van de doorgaande balken niet kan worden verwaarloosd om goede overeenstemming te verkrijgen tussen de gemeten en berekende waarden.